PHYSICAL REVIEW D **96,** 095036 (2017)

Precision tests and fine tuning in twin Higgs models

Roberto Contino,[1,*] Davide Greco,[2,†] Rakhi Mahbubani,[3,‡] Riccardo Rattazzi,[2,§] and Riccardo Torre[2,‖]

[1]*Scuola Normale Superiore and INFN, Pisa IT-56125, Italy*

[2]*Theoretical Particle Physics Laboratory, Institute of Physics, EPFL, Lausanne CH-1015, Switzerland*

[3]*Theoretical Physics Department, CERN, Geneva CH-1211, Switzerland*

(Received 27 February 2017; revised manuscript received 7 November 2017; published 29 November 2017)

We analyze the parametric structure of twin Higgs (TH) theories and assess the gain in fine tuning which they enable compared to extensions of the standard model with colored top partners. Estimates show that, at least in the simplest realizations of the TH idea, the separation between the mass of new colored particles and the electroweak scale is controlled by the coupling strength of the underlying UV theory, and that a parametric gain is achieved only for strongly-coupled dynamics. Motivated by this consideration we focus on one of these simple realizations, namely composite TH theories, and study how well such constructions can reproduce electroweak precision data. The most important effect of the twin states is found to be the infrared contribution to the Higgs quartic coupling, while direct corrections to electroweak observables are subleading and negligible. We perform a careful fit to the electroweak data including the leading-logarithmic corrections to the Higgs quartic up to three loops. Our analysis shows that agreement with electroweak precision tests can be achieved with only a moderate amount of tuning, in the range 5%–10%, in theories where colored states have mass of order 3–5 TeV and are thus out of reach of the LHC. For these levels of tuning, larger masses are excluded by a perturbativity bound, which makes these theories possibly discoverable, hence falsifiable, at a future 100 TeV collider.

DOI: 10.1103/PhysRevD.96.095036

I. INTRODUCTION

The principle of naturalness offers arguably the main motivation for exploring physics at around the weak scale. According to naturalness, the plausibility of specific parameter choices in quantum field theory must be assessed using symmetries and selection rules. When viewing the standard model (SM) as an effective field theory valid below a physical cutoff scale and considering only the known interactions of the Higgs boson, we expect the following corrections to its mass.[1]

$$\delta m_h^2 = \frac{3y_t^2}{4\pi^2}\Lambda_t^2 - \frac{9g_2^2}{32\pi^2}\Lambda_{g_2}^2 - \frac{3g_1^2}{32\pi^2}\Lambda_{g_1}^2 - \frac{3\lambda_h}{8\pi^2}\Lambda_h^2 + \cdots, \tag{1.1}$$

where each Λ represents the physical cutoff scale in a different sector of the theory. The above equation is simply dictated by symmetry: dilatations (dimensional analysis) determine the scale dependence and the broken shift symmetry of the Higgs field sets the coupling dependence. Unsurprisingly, these contributions arise in any explicit UV completion of the SM, although in some cases there may be other larger ones. According to Eq. (1.1), any given (large) value of the scale of new physics can be associated with a (small) number ϵ, which characterizes the accuracy at which the different contributions to the mass must cancel among themselves, in order to reproduce the observed value $m_h \simeq 125$ GeV. As the largest loop factor is due to the top Yukawa coupling, according to Eq. (1.1) the scale Λ_{NP} where new states must first appear is related to m_h^2 and ϵ via

$$\Lambda_{NP}^2 \sim \frac{4\pi^2}{3y_t^2} \times \frac{m_h^2}{\epsilon} \Rightarrow \Lambda_{NP} \sim 0.45\sqrt{\frac{1}{\epsilon}}\text{TeV}. \tag{1.2}$$

The dimensionless quantity ϵ measures how finely-tuned m_h^2 is, given Λ_{NP}, and can therefore be regarded as a measure of the tuning. Notice that the contributions from g_2^2 and λ_h in Eq. (1.1) correspond to $\Lambda_{NP} = 1.1\ \text{TeV}/\sqrt{\epsilon}$ and $\Lambda_{NP} = 1.3\ \text{TeV}/\sqrt{\epsilon}$, respectively. Although not significantly different from the relation in the top sector, these scales would still be large enough to push new states out of direct reach of the LHC for $\epsilon \sim 0.1$.

Indeed, for a given ϵ, Eq. (1.2) only provides an upper bound for Λ_{NP}; in the more fundamental UV theory there

*roberto.contino@sns.it
†davide.greco@epfl.ch
‡rakhi.mahbubani@cern.ch
§riccardo.rattazzi@epfl.ch
‖riccardo.torre@epfl.ch

[1]We take $m_h^2 = 2m_H^2 = \lambda_h v^2/2$ with $\langle H \rangle = v/\sqrt{2} = 174$ GeV, which corresponds to a potential

$$V = -m_H^2|H|^2 + \frac{\lambda_h}{4}|H|^4.$$

can in principle exist larger corrections to m_h^2 which are not captured by Eq. (1.1). In particular, in the minimal supersymmetric SM (MSSM) with high-scale mediation of the soft terms, δm_h^2 in Eq. (1.1) is logarithmically enhanced by RG evolution above the weak scale. In that case, Eq. (1.2) is modified as follows:

$$\Lambda_{NP}^2 \sim \frac{2\pi^2}{3y_t^2} \times \frac{1}{\ln \Lambda_{\rm UV}/\Lambda_{NP}} \times \frac{m_h^2}{\epsilon}, \tag{1.3}$$

where Λ_{NP} corresponds to the overall mass of the stops and $\Lambda_{\rm UV} \gg \Lambda_{NP}$ is the scale of mediation of the soft terms. However, for generic composite Higgs (CH) models, as well as for supersymmetric models with low-scale mediation, Eq. (1.2) provides a fair estimate of the relation between the scale of new physics and the amount of tuning, the Higgs mass being fully generated by quantum corrections at around the weak scale. If the origin of m_h is normally termed *soft* in the MSMM with large $\Lambda_{\rm UV}$ [Eq. (1.3)], it should then be termed *supersoft* in models respecting Eq. (1.2). As is well known, and shown by Eq. (1.3), the natural expectation in the MSSM for $\Lambda_{\rm UV} \gtrsim 100$ TeV is $\Lambda_{NP} \sim m_Z \sim m_h$. In view of this, soft scenarios were already somewhat constrained by direct searches at LEP and Tevatron, whereas the natural range of the scale of supersoft models is only now being probed at the LHC.

Equation (1.2) sets an absolute upper bound on Λ_{NP} for a given fine tuning ϵ, but does not give any information on its nature. In particular it does not specify the quantum numbers of the new states that enter the theory at or below this scale. Indeed, the most relevant states associated with the top sector, the so-called top partners, are bosonic in standard supersymmetric models and fermionic in CH models. Nonetheless, one common feature of these standard scenarios is that the top partners carry SM quantum numbers, color in particular. They are thus copiously produced in hadronic collisions, making the LHC a good probe of these scenarios. Yet there remains the logical possibility that the states that are primarily responsible for the origin of the Higgs mass at or below Λ_{NP} are not charged under the SM, and thus much harder to produce and detect at the LHC. The twin Higgs (TH) is probably the most interesting of the (few) ideas that take this approach [1–22]. This is primarily because the TH mechanism can, at least in principle, be implemented in a SM extension valid up to ultrahigh scales. The structure of TH models is such that the states at the threshold Λ_{NP} in Eq. (1.2) carry quantum numbers under the gauge group of a copy, a twin, of the SM, but are neutral under the SM gauge group. These twin states, of which the twin tops are particularly relevant, are thus poorly produced at the LHC. The theory must also contain states with SM quantum numbers, but their mass m_* is boosted with respect to Λ_{NP} roughly by a factor $g_*/g_{\rm SM}$, where g_* describes the coupling strength of the new dynamics, while $g_{\rm SM}$ represents a generic SM coupling. As discussed in the next section, depending on the structure of the model, $g_{\rm SM}$ can be either the top Yukawa or the square root of the Higgs quartic. As a result, given the tuning ϵ, the squared mass of the new colored and charged states is roughly given by

$$m_*^2 \sim \frac{4\pi^2}{3y_t^2} \times \frac{m_h^2}{\epsilon} \times \left(\frac{g_*}{g_{\rm SM}}\right)^2. \tag{1.4}$$

For $g_* > g_{\rm SM}$, we could define these model as effectively *hypersoft*, in that, for fixed fine tuning, the gap between the SM-charged states and the weak scale is even larger than that in supersoft models. In practice the above equation implies that, for strong g_*, the new states are out of reach of the LHC even for mild tuning (see Sec. II A for a more precise statement). Equation (1.4) synthesizes the potential relevance of the TH mechanism, and makes it clear that the new dynamics must be rather strong for the mechanism to work. Given the hierarchy problem, it then seems almost inevitable to make the TH a composite TH (although it could also be a supersymmetric composite TH). Realizations of the TH mechanism within the paradigm of CH models with fermion partial compositeness [23] have already been proposed, both in the holographic and effective theory setups [6,9,13,14].

It is important to recognize that the factor that boosts the mass of the states with SM gauge quantum numbers in Eq. (1.4) is the coupling g_* itself. Because of this, strong-dynamics effects in the Higgs sector, which are described in the low-energy theory by nonrenormalizable operators with coefficients proportional to powers of g_*/m_*, do not "decouple" when these states are made heavier, at fixed fine tuning ϵ. In the standard parametrics of the CH, m_*/g_* is of the order of f, the decay constant of the σ-model within which the Higgs doublet emerges as a pseudo-Nambu-Goldstone boson (pNGB). Then $\xi \equiv v^2/f^2$, as well as being a measure of the fine tuning through $\epsilon = 2\xi$, also measures the relative deviation of the Higgs couplings from the SM ones, in the TH like in any CH model.[2] Recent Higgs coupling measurements roughly constrain $\xi \lesssim$ 10–20% [24], and a sensitivity of order 5% is expected in the high-luminosity phase of the LHC [25]. However Higgs loop effects in precision Z-pole observables measured at LEP already limit $\xi \lesssim 5\%$ [26,27]. Having to live with this few-percent tuning would somewhat undermine the motivation for the clever TH construction. In ordinary CH models this strong constraint on ξ can in principle be relaxed thanks to compensating corrections to the $\hat{T}$ parameter coming from the top partners. In the most natural models, these are proportional to $y_t^4 v^2/m_*^2$ and thus, unlike the Higgs-sector contribution, decouple when m_* is

[2]The factor of two difference between the fine tuning ϵ and ξ is due to the Z_2 symmetry of the Higgs potential in the TH models, as shown in Sec. II A [7].

increased. This makes it hard to realize such a compensatory effect in the most distinctive range of parameters for TH models, where $m_* \sim 5$–10 TeV. Alternatively one could consider including custodial-breaking couplings larger than y_t in the top-partner sector. Unfortunately these give rise to equally-enhanced contributions to the Higgs potential, which would in turn require further ad-hoc cancellations.

As already observed in the literature [13,14] another important aspect of TH models is that calculable IR-dominated contributions to the Higgs quartic coupling almost saturate its observed value. Though a welcome property in principle, this sets even stronger constraints on additional UV contributions, such as those induced by extra sources of custodial breaking. In this paper we study the correlation between these effects, in order to better assess the relevance of the TH construction as a valid alternative to more standard ideas about EW-scale physics. Several such studies already exist for standard composite Higgs scenarios [28–30]. In extending these to the TH we shall encounter an additional obstacle to gaining full benefit from the TH boost in Eq. (1.4): the model structure requires rather "big" multiplets, implying a large number of degrees of freedom. This results in an upper bound for the coupling that is parametrically smaller than 4π by naive dimensional analysis (NDA); hence the boost factor is similarly depressed. We shall discuss in detail how serious and unavoidable a limitation this is.

The paper is organized as follows: in Sec. II we discuss the general structure and parametrics of TH models, followed by Sec. III where we discuss the more specific class of composite TH models we focus on for the purpose of our study. In Secs. IV and V we present our computations of the basic physical quantities: the Higgs potential and precision electroweak parameters ($\hat{S}, \hat{T}, \delta g_{Lb}$). Section VI is devoted to a discussion of the resulting constraints on the model and an appraisal of the whole TH scenario. Our conclusions are presented in Sec. VII.

II. THE TWIN HIGGS SCENARIO

A. Structure and parametrics

In this section we outline the essential aspects of the TH mechanism. Up to details and variants which are not crucial for the present discussion, the TH scenario involves an exact duplicate, $\widetilde{\mathrm{SM}}$, of the SM fields and interactions, underpinned by a Z_2 symmetry. In practice this Z_2 must be explicitly broken in order to obtain a realistic phenomenology, and perhaps more importantly, a realistic cosmology [19–21]. However the sources of Z_2 breaking can have a structure and size that makes them irrelevant in the discussion of naturalness in electroweak symmetry breaking, which is the main goal of this section.

Our basic assumption is that the SM and its twin emerge from a more fundamental Z_2-symmetric theory at the scale m_*, at which new states with SM quantum numbers, color in particular, first appear. In order to get a feel for the mechanism and its parametrics, it is sufficient to focus on the most general potential for two Higgs doublets H and $\tilde{H}$, invariant under the gauge group $G_{\mathrm{SM}} \times \tilde{G}_{\mathrm{SM}}$, with $G_{\mathrm{SM}} = SU(3)_c \times SU(2)_L \times U(1)_Y$, as well as a Z_2:

$$V(H,\tilde{H}) = -m_{\mathcal{H}}^2(|H|^2 + |\tilde{H}|^2) + \frac{\lambda_{\mathcal{H}}}{4}(|H|^2 + |\tilde{H}|^2)^2 + \frac{\hat{\lambda}_h}{8}(|H|^4 + |\tilde{H}|^4). \tag{2.1}$$

Strictly speaking, the above potential does not have minima with realistic "tunable" $\langle H \rangle$. This goal can be achieved by the simple addition of a naturally small Z_2-breaking mass term which, while changing the vacuum expectation value, does not affect the estimates of fine tuning, and hence will be neglected for the purposes of this discussion. Like for the SM Higgs, the most general potential is accidentally invariant under a custodial $SO(4) \times \widetilde{SO}(4)$. Notice however that in the limit $\hat{\lambda}_h \to 0$, the additional Z_2 enhances the custodial symmetry to $SO(8)$, where $\mathcal{H} \equiv H \oplus \tilde{H} \equiv \mathbf{8}$. In this exact limit, if $\tilde{H}$ acquired an expectation value $\langle \tilde{H} \rangle \equiv f/\sqrt{2}$, all 4 components of the ordinary Higgs H would remain exactly massless NGBs. Of course the SM and $\widetilde{\mathrm{SM}}$ gauge and Yukawa couplings, along with $\hat{\lambda}_h$, explicitly break the $SO(8)$ symmetry that protects the Higgs. Consider however the scenario where these other couplings, which are known to be weak, can be treated as small $SO(8)$-breaking perturbations of a stronger $SO(8)$-preserving underlying dynamics, of which the quartic coupling $\lambda_{\mathcal{H}}$ is a manifestation. In this situation we can reassess the relation between the SM Higgs mass, the amount of tuning and the scale m_* where new states charged under the SM are first encountered, treating $\hat{\lambda}_h$ as a small perturbation of $\lambda_{\mathcal{H}}$. At zeroth order, i.e., neglecting $\hat{\lambda}_h$, we can expand around the vacuum $\langle \tilde{H} \rangle^2 = 2m_{\mathcal{H}}^2/\lambda_{\mathcal{H}} \equiv f^2/2$, $\langle H \rangle = 0$. The spectrum consists of a heavy scalar σ, with mass $m_\sigma = \sqrt{2} m_{\mathcal{H}} = \sqrt{\lambda_{\mathcal{H}}} f/\sqrt{2}$, corresponding to the radial mode, 3 NGBs eaten by the twin gauge bosons, which get masses $\sim gf/2$ and the massless H. When turning on $\hat{\lambda}_h$, $SO(8)$ is broken explicitly and H acquires a potential. At leading order in a $\hat{\lambda}_h/\lambda_{\mathcal{H}}$ expansion the result is simply given by substituting $|\tilde{H}|^2 = f^2/2 - |H|^2$ in Eq. (2.1).[3] The quartic coupling and the correction to the squared mass are then given by

$$\lambda_h \simeq \hat{\lambda}_h \qquad \delta m_H^2 \sim \hat{\lambda}_h f^2/8 \simeq (\lambda_h/2\lambda_{\mathcal{H}}) m_{\mathcal{H}}^2. \tag{2.2}$$

[3]Notice that the effective Higgs quartic receives approximately equal contributions from $|H|^4$ and $|\tilde{H}|^4$. This is a well-known and interesting property of the TH, see for instance Ref. [7].

As mentioned above, we assume that m_H^2 also receives an independent contribution from a Z_2-breaking mass term, which can be ignored in the estimates of tuning. Note that in terms of the physical masses of the Higgs, m_h, and of its heavy twin, m_σ, we have precisely the same numerical relation $\delta m_h^2 = (\lambda_h/2\lambda_\mathcal{H}) m_\sigma^2$. The amount of tuning ϵ, defined as $m_h^2/\delta m_h^2$, is given by $\epsilon = 2\xi = 2v^2/f^2$.

Our estimate of δm_H^2 in Eq. (2.2) is based on a simplifying approximation where the $SO(8)$-breaking quartic is taken Z_2-symmetric. In general we could allow different couplings $\hat{\lambda}_h$ and $\hat{\lambda}_{\tilde{h}}$ for $|H|^4$ and $|\tilde{H}|^4$ respectively, constrained by the requirement $\hat{\lambda}_h + \hat{\lambda}_{\tilde{h}} \simeq 2\lambda_h$. As the estimate of δm_H^2 in Eq. (2.2) is determined by the $|\tilde{H}|^4$ term, it is clear that a reduction of $\hat{\lambda}_{\tilde{h}}$, with λ_h fixed, would improve the tuning, as emphasized in Ref. [22]. As discussed in Sec. IV, however, a significant fraction of the contribution to $\hat{\lambda}_h$ and $\hat{\lambda}_{\tilde{h}}$ is coming from RG evolution due to the top and twin top. According to our analysis, $\hat{\lambda}_h/\hat{\lambda}_{\tilde{h}}$ varies between 1.5 in the simplest models to 3 in models where $\hat{\lambda}_{\tilde{h}}$ is purely IR-dominated as in Ref. [22]. Though interesting, this gain does not change our parametric estimates.

The ratio $\lambda_h/\lambda_\mathcal{H}$ is the crucial parameter in the game. Indeed it is through Eq. (2.2) that m_H is sensitive to quantum corrections to the Lagrangian mass parameter $m_\mathcal{H}$, or, equivalently, that the physical Higgs mass m_h is sensitive to the physical mass of the radial mode m_σ. In particular, what matters is the correlation of m_σ with, and its sensitivity to, m_*, where new states with SM quantum numbers appear. One can think of three basic scenarios for that relation, which we now illustrate, ordering them by increasing level of model-building ingenuity. Beyond these scenarios there is the option of tadpole-dominated electroweak symmetry breaking, which we shall briefly discuss at the end.

1. Subhypersoft scenario

The simplest option is given by models with $m_\sigma \sim m_*$. Supersymmetric TH models with medium- to high-scale soft-term mediation belong to this class [7], with m_* representing the soft mass of the squarks. Like in the MSSM, $m_\mathcal{H}$, and therefore m_σ, is generated via RG evolution: two decades of running are sufficient to obtain $m_\sigma \sim m_*$. Another example is composite TH models [13,14]. In their simplest incarnation they are characterized by one overall mass scale m_* and coupling g_* [31], so that by construction one has $m_\sigma \sim m_*$ and $\lambda_\mathcal{H} \sim g_*^2$. As discussed below Eq. (2.2), in both these scenarios one then expects $\delta m_h^2 \sim (\lambda_h/2\lambda_\mathcal{H}) m_*^2$. It is interesting to compare this result to the leading top-sector contribution in Eq. (1.1). For that purpose it is worth noticing that, as discussed in Sec. IV, in TH models the RG-induced contribution to the Higgs quartic coupling $\Delta\lambda_h|_{RG} \sim (3y_t^4/\pi^2) \ln m_*/m_t$ (more than) saturates its experimental value $\lambda_h \sim 0.5$ for $m_* \sim 3$–10 TeV.[4] We can thus write

$$\delta m_h^2 \sim (\lambda_h/2\lambda_\mathcal{H}) m_*^2 \sim \frac{3y_t^4}{2\pi^2}\frac{1}{\lambda_\mathcal{H}} \ln(m_*/m_t) m_*^2 \equiv \frac{3y_t^2}{2\pi^2} \times \frac{y_t^2}{g_*^2} \times \ln(m_*/m_t) \times m_*^2 \tag{2.3}$$

which should be compared to the first term on the right-hand side of Eq. (1.1). Accounting for the possibility of tuning we then have

$$m_* \sim 0.45 \times \frac{g_*}{\sqrt{2}y_t} \times \sqrt{\frac{1}{\ln(m_*/m_t)}} \times \sqrt{\frac{1}{\epsilon}}\ \text{TeV}. \tag{2.4}$$

Compared to Eq. (1.2), the mass of colored states is on one hand parametrically boosted by the ratio $g_*/(\sqrt{2}y_t)$, and on the other it is mildly decreased by the logarithm. The motivation for, and gain in, the ongoing work on the simplest realization of the TH idea pivot upon the above g_*/y_t. The basic question is how high g_* can be pushed without leading to a breakdown of the effective description. One goal of this paper is to investigate to what extent one can realistically gain from this parameter in more explicit CH realizations. Applying naive dimensional analysis (NDA) one would be tempted to say that g_* as big as $\sim 4\pi$ makes sense, in which case $m_* \sim 10$ TeV would only cost a mild $\epsilon \sim 0.1$ tuning. However such an estimate seems quantitatively too naive. For instance, by focusing on the simple toy model whose potential is given by Eq. (2.1), we can associate the upper bound on $\lambda_\mathcal{H} \equiv g_*^2$, to the point where perturbation theory breaks down. One possible way to proceed is to consider the one loop beta function

$$\mu \frac{d\lambda_\mathcal{H}}{d\mu} = \frac{N+8}{32\pi^2}\lambda_\mathcal{H}^2, \tag{2.5}$$

and to estimate the maximum value of the coupling $\lambda_\mathcal{H}$ as that for which $\Delta\lambda_\mathcal{H}/\lambda_\mathcal{H} \sim O(1)$ through one e-folding of RG evolution. We find

$$\lambda_\mathcal{H} = \frac{2m_\sigma^2}{f^2} \lesssim \frac{32\pi^2}{N+8} \Rightarrow \frac{m_\sigma}{f} \lesssim \pi, \qquad \text{for } N = 8, \tag{2.6}$$

which also gives $g_* \sim \sqrt{\lambda_\mathcal{H}} \lesssim \sqrt{2}\pi$, corresponding to a significantly smaller maximal gain in Eq. (2.4) with respect to the NDA estimate. In Sec. III B we shall perform alternative estimates in more specific CH constructions, obtaining similar results.

[4]For this naive estimate we have taken the twin-top contribution equal to the top one, so that the result is just twice the SM one. For a more precise statement see Sec. IV.

It is perhaps too narrow-minded to stick rigidly to such estimates to determine the boost that $g_*/(\sqrt{2}y_t)$ can give to m_*. Although it is parametrically true that the stronger the coupling g_*, the heavier the colored partners can be at fixed tuning, the above debate over factors of a few make it difficult to be more specific in our estimates. In any case the gain permitted by Eq. (2.4) is probably less than one might naively have hoped, making it fair to question the motivation for the TH, at least in its "subhypersoft" realization. With this reservation in mind, we continue our exploration of the TH in the belief that the connection between naturalness and LHC signatures is so crucial that it must be analyzed in all its possible guises.

Concerning in particular composite TH scenarios one last important model building issue concerns the origin of the Higgs quartic λ_h. In generic CH it is known that the contribution to λ_h that arises at $O(y_t^2)$ is too large when g_* is strong. Given that the TH mechanism demands g_* as strong as possible then composite TH models must ensure that the leading $O(y_t^2)$ contribution is absent so that λ_h arises at $O(y_t^4)$. As discussed in Ref. [13], this property is not guaranteed but it can be easily ensured provided the couplings that give rise to y_t via partial compositeness respect specific selection rules.

2. Hypersoft scenario

The second option corresponds to the structurally robust situation where m_σ^2 is one loop factor smaller than m_*^2. This is for instance achieved if $\mathcal{H}$ is a PNG-boson octet multiplet associated to the spontaneous breaking $SO(9) \to SO(8)$ in a model with fundamental scale m_*. Another option would be to have a supersymmetric model where supersymmetric masses of order m_* are mediated to the stops at the very scale m_* at which $\mathcal{H}$ is massless. Of course in both cases a precise computation of m_σ^2 would require the full theory. However a parametrically correct estimate can be given by considering the quadratically divergent 1-loop corrections in the low energy theory, in the same spirit of Eq. (1.1). As y_t and $\lambda_\mathcal{H}$ are expected to be the dominant couplings the analogue of Eqs. (1.1) and (2.2) imply

$$\delta m_h^2 \sim \frac{\lambda_h}{2\lambda_\mathcal{H}}\left(\frac{3y_t^2}{4\pi^2}+\frac{5\lambda_\mathcal{H}}{16\pi^2}\right)m_*^2 = \left(\frac{y_t^2}{\lambda_\mathcal{H}}+\frac{5}{12}\right)\frac{3\lambda_h}{8\pi^2}m_*^2. \tag{2.7}$$

Very roughly, for $\lambda_\mathcal{H} \gtrsim y_t^2$, top effects become subdominant and the natural value for m_h becomes controlled by λ_h, like the term induced by the Higgs quartic in Eq. (1.1). In the absence of tuning this roughly corresponds to the technicolor limit $m_* \sim 4\pi v$, while allowing for fine tuning we have

$$m_* \sim 1.4 \times \sqrt{\frac{1}{\epsilon}}\ \text{TeV}. \tag{2.8}$$

It should be said that in this scenario there is no extra boost of m_* at fixed tuning by taking $\lambda_\mathcal{H} > y_t^2$. Indeed the choice $\lambda_\mathcal{H} \sim y_t^2$ is preferable as concerns electroweak precision tests (EWPT). It is well known that RG evolution in the effective theory below m_σ gives rise to corrections to the $\hat{S}$ and $\hat{T}$ parameters as discussed in Sec. V [32]. In view of the relation $\epsilon = 2v^2/f^2$ this gives a direct connection between fine-tuning electroweak precision data, and the mass of the twin Higgs m_σ. At fixed v^2/f^2, EWPT then favor the smallest possible $m_\sigma = \sqrt{\lambda_\mathcal{H}} f/\sqrt{2}$, that is the smallest $\lambda_\mathcal{H} \sim y_t^2$. The most plausible spectrum in this class of models is roughly the following: the twin scalar σ and the twin tops appear around the same scale $\sim y_t f/\sqrt{2}$, below the colored partners who live at m_*. The presence of the somewhat light scalar σ is one of interesting features of this class of models.

3. Superhypersoft scenario

This option is a clever variant of the previous one, where below the scale m_* approximate supersymmetry survives in the Higgs sector in such a way that the leading contribution to $\delta m_\mathcal{H}^2$ proportional to $\lambda_\mathcal{H}$ is purely due to the top sector [7]. In that way Eq. (2.7) reduces to

$$\delta m_h^2 \sim \frac{\lambda_h}{2\lambda_\mathcal{H}}\left(\frac{3y_t^2}{4\pi^2}\right)m_*^2 = \frac{y_t^2}{\lambda_\mathcal{H}} \times \frac{3\lambda_h}{8\pi^2}m_*^2. \tag{2.9}$$

so that by choosing $g_* > y_t$ one can push the scale m_* further up with fixed fine tuning ϵ

$$m_* \sim 1.4 \times \frac{g_*}{\sqrt{2}y_t} \times \sqrt{\frac{1}{\epsilon}}\ \text{TeV}. \tag{2.10}$$

In principle even under the conservative assumption that $g_* \sim \sqrt{2}\pi$ is the maximal allowed value, this scenario seemingly allows $m_* \sim 14$ TeV with a mild $\epsilon \sim 0.1$ tuning.

It should be said that in order to realize this scenario one would need to complete $\mathcal{H}$ into a pair of chiral superfield octets $\mathcal{H}_u$ and $\mathcal{H}_d$, along the lines of Ref. [7], as well as add a singlet superfield S in order to generate the Higgs quartic via the superpotential trilinear $g_* S \mathcal{H}_u \mathcal{H}_d$. Obviously this is a very far-fetched scenario combining all possible ideas to explain the smallness of the weak scale: supersymmetry, compositeness, and the twin Higgs mechanism.

4. Alternative vacuum dynamics: Tadpole induced EWSB

In all the scenarios discussed so far the tuning of the Higgs vacuum expectation value (VEV) and that of the Higgs mass coincided: ϵ, which controls the tuning of m_h^2 according to Eqs. (2.4), (2.8), and (2.10), is equal to $2v^2/f^2$, which measures the tuning of the VEV. This was because the only tuning in the Higgs potential was associated with the small quadratic term, while the quartic

was assumed to be of the right size without the need for further cancellations (see, e.g., the discussion in Ref. [33]). Experimentally however, one can distinguish between the need for tuning that originates from measurements of Higgs and electroweak observables, which are controlled by v^2/f^2, and that coming from direct searches for top partners. Currently, with bounds on colored top partners at just around 1 TeV [34,35], but with Higgs couplings already bounded to lie within 10%–20% of their SM value [24], the only reason for tuning in all TH scenarios is to achieve a small v^2/f^2. It is then fair to consider options that reduce or eliminate only the tuning of v^2/f^2. As argued in Ref. [18], this can be achieved by modifying the H scalar vacuum dynamics, and having its VEV induced instead by a tadpole mixing with an additional electroweak-breaking technicolor (TC) sector [36–38]. In order to preserve the Z_2 symmetry one adds two twin TC sectors, both characterized by a mass scale m_{TC} and a decay constant $f_{TC} \sim m_{TC}/4\pi$ (i.e., it is parametrically convenient to assume $g_{TC} \sim 4\pi$). Below the TC scale the dynamics in the visible and twin sectors is complemented by Goldstone triplets π_a and $\tilde{\pi}_a$ which can be embedded into doublet fields according to

$$\Sigma = f_{TC} e^{i\pi_a \sigma_a} \begin{pmatrix} 0 \\ 1 \end{pmatrix}, \qquad \tilde{\Sigma} = f_{TC} e^{i\tilde{\pi}_a \sigma_a} \begin{pmatrix} 0 \\ 1 \end{pmatrix}, \quad (2.11)$$

and are assumed to mix with H and $\tilde{H}$ via the effective potential terms

$$V_{\text{tadpole}} = M^2 (H^\dagger \Sigma + \tilde{H}^\dagger \tilde{\Sigma}) + \text{H.c.} \quad (2.12)$$

Assuming $m_{TC} \ll m_{\mathcal{H}}$ the $\tilde{H}$ vacuum dynamics is not significantly modified, but, for $m_{TC} > m_h$, V_{tadpole} acts like a rigid tadpole term for H. The expectation value $\langle H \rangle$ is thus determined by balancing such a tadpole against the gauge-invariant $|H|^2$ mass term; the latter will then roughly coincide with m_h^2. In order for this to work, by Eq. (2.2) the $SO(8)$-breaking quartic $\hat{\lambda}_h$ should be negative, resulting in $v \sim (M^2/m_h^2) f_{TC}$. It is easy to convince oneself that the corrections to Higgs couplings are $O(f_{TC}^2/v^2)$: present bounds can then be satisfied for $f_{TC} \sim v/\sqrt{10} \simeq 80$ GeV. In turn, the value of v/f is controlled by f and can thus be naturally small. The TC scale is roughly $m_{TC} \sim 4\pi f_{TC} \sim$ 600–800 GeV, while the noneaten pNGB π in Eq. (2.11) have a mass $m_\pi^2 \sim M^2 v/f_{TC} \sim m_h^2 (v/f_{TC})^2 \sim 400$ GeV. The latter value, although rather low, is probably large enough to satisfy constraints from direct searches. In our opinion, what may be more problematic are EWPT, in view of the effects from the TC sector, which shares some of the vices of ordinary TC. The IR contributions to $\hat{S}$ and $\hat{T}$, associated with the splitting $m_{\pi_a} < m_{TC}$, are here smaller than the analogues of ordinary technicolor (there associated with the splitting $m_W \ll m_{TC}$). However the UV contribution to $\hat{S}$ is parametrically the same as in ordinary TC, in particular it is enhanced at large N_{TC}. Even at $N_{TC} = 2$, staying within the allowed $(\hat{S}, \hat{T})$ ellipse still requires a correlated contribution from $\Delta\hat{T}$, which in principle should also be counted as tuning. In spite of this, models with tadpole-induced EWSB represent a clever variant where, technically, the dynamics of EWSB does not currently appear tuned. A thorough analysis of the constraints is certainly warranted.

III. THE COMPOSITE TWIN HIGGS

In this section and in the remainder of the paper, we will focus on the CH realization of the TH, which belongs to the subhypersoft class of models. In this simple and well-motivated context we shall discuss EWPT, fine tuning, and structural consistency of the model.

Our basic structural assumption is that at a generic UV scale $\Lambda_{\text{UV}} \gg m_*$, our theory can be decomposed into two sectors: a strongly-interacting composite sector and a weakly-interacting elementary sector. The composite sector is assumed to be endowed with the global symmetry $G = SO(8) \times U(1)_X \times Z_2$ and to be approximately scale-(conformal) invariant down to the scale m_*, at which it develops a mass gap. We assume the overall interaction strength at the resonance mass scale m_* to be roughly described by one parameter g_* [31]. The large separation of mass scales $\Lambda_{\text{UV}} \gg m_*$ is assumed to arise naturally, in that the occurrence of the mass gap m_* is controlled by either a marginally relevant deformation, or by a relevant deformation whose smallness is controlled by some global symmetry. At the scale m_*, $SO(8) \times U(1)_X \times Z_2$ is spontaneously broken to the subgroup $H = SO(7) \times U(1)_X$, giving rise to seven NGBs in the **7** of $SO(7)$ with decay constant $f \sim m_*/g_*$. The subgroup $U(1)_X$ does not participate to the spontaneous breaking, but its presence is needed to reproduce the hypercharges of the SM fermions, similarly to CH models. The elementary sector consists in turn of two separate weakly interacting sectors: one containing the visible SM fermions and gauge bosons, corresponding to the SM gauge group $G_{\text{SM}} = SU(3)_c \times SU(2)_L \times U(1)_Y$; the other containing the twin SM with the same fermion content and a $\widetilde{\text{SM}}$ gauge group $\tilde{G}_{\text{SM}} = \widetilde{SU}(3)_c \times \widetilde{SU}(2)_L$. The external Z_2 symmetry, or twin parity, interchanges these two copies. For simplicity, and following [13], we choose not to introduce a mirror hypercharge field. This is our only source of explicit twin-parity breaking, and affects neither our discussion of fine tuning, nor that of precision electroweak measurements.

The elementary and composite sectors are coupled according to the paradigm of partial compositeness [23]. The elementary EW gauge bosons couple to the strong dynamics as a result of the weak gauging of the $SU(2)_L \times U(1)_Y \times \widetilde{SU}(2)_L$ subgroup of the global $SO(8) \times U(1)_X$. A linear mixing with the global conserved currents is thus induced:

$$\mathcal{L}^V_{\rm mix} \supset g_2 W^\alpha_\mu J^\mu_\alpha + g_1 B_\mu J^\mu_B + \tilde{g}_2 \tilde{W}^\alpha_\mu \tilde{J}^\mu_\alpha, \qquad (3.1)$$

where $g_{1,2}$ and $\tilde{g}_2$ denote the SM and twin weak gauge couplings, $J^\mu_B \equiv J^\mu_{3R} + J^\mu_X$ and J^μ, $\tilde{J}^\mu$ and J^μ_X are the currents associated respectively to the $SU(2)_L$, $\widetilde{SU}(2)_L$ and $U(1)_X$ generators. The elementary fermions mix analogously with various operators transforming as linear representations of $SO(8)$ that are generated in the far UV by the strongly interacting dynamics. The mixing Lagrangian takes the schematic form:

$$\mathcal{L}^F_{\rm mix} \supset \bar{q}^\alpha_L \Delta_{\alpha A} \mathcal{O}^A_R + \bar{t}_R \Theta_A \mathcal{O}^A_L + \bar{\tilde{q}}^\alpha_L \tilde{\Delta}_{\alpha A} \tilde{\mathcal{O}}^A_R + \bar{t}_R \tilde{\Theta}_A \tilde{\mathcal{O}}^A_L + \text{H.c.}, \qquad (3.2)$$

where, following, e.g., Ref. [39], we introduced spurions $\Delta_{\alpha A}$, $\tilde{\Delta}_{\alpha A}$, Θ_A, and $\tilde{\Theta}_A$ in order to uplift the elementary fields to linear representations of $SO(8)$, and match the quantum numbers of the composite operators. The left-handed mixings $\Delta_{\alpha A}$, $\tilde{\Delta}_{\alpha A}$ necessarily break $SO(8)$ since q_L only partially fills a multiplet of $SO(8)$. The right-handed mixings, instead, may or may not break $SO(8)$. The breaking of $SO(8)$ gives rise to a potential for the NGBs at one loop and the physical Higgs is turned into a pNGB. We conclude by noticing that $g_{1,2}$ and $\tilde{g}_2$ correspond to quasimarginal couplings which start off weak in the UV, and remain weak down to m_*. The fermion mixings could be either relevant or marginal, and it is possible that some may correspond to interactions that grow as strong as g_* at the IR scale m_* [40]. In particular, as is well known, there is some advantage as regards tuning in considering the right mixings Θ_A and $\tilde{\Theta}_A$ to be strong. In that case one may even imagine the IR scale to be precisely generated by the corresponding deformation of the fixed point. While this latter option may be interesting from a top-down perspective, it would play no appreciable role in our low-energy phenomenological discussion.

A. A simplified model

In order to proceed we now consider a specific realization of the composite TH and introduce a concrete simplified effective Lagrangian description of its dynamics. Our model captures the most important features of this class of theories, like the pNGB nature of the Higgs field, and provides at the same time a simple framework for the interactions between the elementary fields and the composite states, vectors and fermions. We make use of this effective model as an example of a specific scenario in which we can compute EW observables, and study the feasibility of the TH idea as a new paradigm for physics at the EW scale.

We write down an effective Lagrangian for the composite TH model using the Callan-Coleman-Wess-Zumino (CCWZ) construction [41,42], and generalizing the simpler case of a two-site model developed in Ref. [13]. According to the CCWZ technique, a Lagrangian invariant under the global $SO(8)$ group can be written following the rules of a local $SO(7)$ symmetry. The basic building blocks are the Goldstone matrix $\Sigma(\mathbf{\Pi})$, which encodes the seven NGBs, $\mathbf{\Pi}$, present in the theory, and the operators $d_\mu(\mathbf{\Pi})$ and $E_\mu(\mathbf{\Pi})$ resulting from the Maurer-Cartan form constructed with the Goldstone matrix. An external $U(1)_X$ group is also added to the global invariance in order to reproduce the correct fermion hypercharges [13]. The CCWZ approach is reviewed and applied to the $SO(8)/SO(7)$ coset in Appendix A.

Before proceeding, we would like to recall the simplified model philosophy of Ref. [43], which we essentially employ. In a generic composite theory, the mass scale m_* would control both the cutoff of the low energy σ-model and the mass of the resonances. In that case no effective Lagrangian method is expected to be applicable to describe the resonances. So, in order to produce a manageable effective Lagrangian we thus consider a Lagrangian for resonances that can, at least in principle, be made lighter that m_*. One more structured way to proceed could be to consider a deconstructed extra-dimension where the mass of the lightest resonances, corresponding to the inverse compactification length, is parametrically separated from the 5D cut-off, interpreted as m_*. Here we do not go that far and simply consider a set of resonances that happen to be a bit lighter than m_*. We do so to give a structural dignity to our effective Lagrangian, though at the end, for our numerical analysis, we just take the resonances a factor of 2 below m_*. We believe that is a fair procedure given our purpose of estimating the parametric consistency of the general TH scenario.

We start our analysis of the effective Lagrangian with the bosonic sector. Together with the elementary SM gauge bosons, the W's and B, we introduce the twin partners $\tilde{W}$ to gauge the $\widetilde{SU}(2)_L$ group. As representative of the composite dynamics, we restrict our interest to the heavy spin-1 resonances transforming under the adjoint of $SO(7)$ and to a vector singlet. We therefore introduce a set of vectors ρ^a_μ which form a **21** of $SO(7)$ and the gauge vector associated with the external $U(1)_X$, which we call ρ^X_μ. The Lagrangian for the bosonic sector can be written as

$$\mathcal{L}_{\rm bosonic} = \mathcal{L}_\pi + \mathcal{L}^V_{\rm comp} + \mathcal{L}^V_{\rm elem} + \mathcal{L}^V_{\rm mix}. \qquad (3.3)$$

The first term describes the elementary gauge bosons masses and the NGBs dynamics and is given by

$$\mathcal{L}_\pi = \frac{f^2}{4} \text{Tr}[d_\mu d^\mu]. \qquad (3.4)$$

The second term, $\mathcal{L}^V_{\rm comp}$, is a purely composite term, generated at the scale m_* after confinement; it reduces to the kinetic terms for the ρ vectors, namely:

$$\mathcal{L}^V_{\rm comp} = -\frac{1}{4g_\rho^2}\rho^a_{\mu\nu}\rho^{\mu\nu a} - \frac{1}{4g_{\rho^X}^2}\rho^X_{\mu\nu}\rho^{X\mu\nu}, \tag{3.5}$$

where $\rho^a_{\mu\nu} = \partial_\mu\rho^a_\nu - \partial_\nu\rho^a_\mu - f_{abc}\rho^b_\mu\rho^c_\nu$, $\rho^X_{\mu\nu} = \partial_\mu\rho^X_\nu - \partial_\nu\rho^X_\mu$, and g_ρ and g_{ρ^X} are the coupling strengths for the composite spin-1 bosons. The third term in Eq. (3.3), $\mathcal{L}^V_{\rm elem}$, is a purely elementary interaction, produced at the scale $\Lambda_{\rm UV}$ where the elementary fields are formally introduced. Also this Lagrangian can contain only the kinetic terms for the elementary fields:

$$\mathcal{L}^V_{\rm elem} = -\frac{1}{4g_1^2}B_{\mu\nu}B^{\mu\nu} - \frac{1}{4g_2^2}W^a_{\mu\nu}W^{a\mu\nu} - \frac{1}{4\tilde{g}_2^2}\tilde{W}^a_{\mu\nu}\tilde{W}^{a\mu\nu}, \tag{3.6}$$

where g_1, g_2, and $\tilde{g}_2$ denote the weak gauge couplings. The last term in the Lagrangian (3.3), $\mathcal{L}^V_{\rm mix}$, is a mixing term between the elementary and composite sectors originating from partial compositeness. We have:[5]

$$\mathcal{L}^V_{\rm mix} = \frac{M_\rho^2}{2g_\rho^2}(\mathrm{Tr}[\rho^a_\mu T^{\mathbf{21}}_a - E_\mu])^2 + \frac{M_{\rho^X}^2}{2g_{\rho^X}^2}(\rho^X_\mu - B_\mu)^2, \tag{3.7}$$

where $T^{\mathbf{21}}_a$ are the $SO(8)$ generators in the adjoint of $SO(7)$ (see Appendix A).

We now introduce the Lagrangian for the fermionic sector. This depends on the choice of quantum numbers for the composite operators in Eq. (3.2). The minimal option is to choose $\mathcal{O}_R$ and $\tilde{\mathcal{O}}_R$ to be in the fundamental representation of $SO(8)$, whereas the operators $\mathcal{O}_L$ and $\tilde{\mathcal{O}}_L$ are singlets of the global group. Therefore, the elementary SM doublet and its twin must be embedded into fundamental representations of $SO(8)$, whereas the t_R and the $\tilde{t}_R$ are complete singlets under the global $SO(8)$ invariance. This choice is particularly useful to generalize our discussion to the case of a fully-composite right-handed top. From the low-energy perspective, the linear mixing between composite operators and elementary fields translates into a linear coupling between the latter and a layer of fermionic resonances excited from the vacuum by the operators in the fundamental and singlet representations of the global group. Decomposing the **8** of $SO(8)$ as $\mathbf{8} = \mathbf{7} + \mathbf{1}$ under $SO(7)$, we introduce a set of fermionic resonances filling a complete fundamental representation of $SO(7)$ and another set consisting of just one singlet.[6] We denote with $\Psi_{\mathbf{7}}$ the fermionic resonances in the septuplet and with $\Psi_{\mathbf{1}}$ the singlet, both charged under $SU(3)_c$. Together with them, we must introduce analogous composite states charged under $\widetilde{SU}(3)_c$; we use the corresponding notation $\tilde{\Psi}_{\mathbf{7}}$ and $\tilde{\Psi}_{\mathbf{1}}$. We refer to Ref. [13] for the complete expression of $\Psi_{\mathbf{7}}$ and $\tilde{\Psi}_{\mathbf{7}}$ in terms of the constituent fermions.

The fermionic effective Lagrangian is split into three parts, which have the same meaning as the analogous distinctions we made for the bosonic sector of the theory:

$$\mathcal{L}_{\rm fermionic} = \mathcal{L}^F_{\rm comp} + \mathcal{L}^F_{\rm elem} + \mathcal{L}^F_{\rm mix}. \tag{3.8}$$

The fully composite term is given by:

$$\begin{aligned}\mathcal{L}^F_{\rm comp} = {}& \bar{\Psi}_{\mathbf{7}}(i\not{D}_{\mathbf{7}} - M_\Psi)\Psi_{\mathbf{7}} + \bar{\Psi}_{\mathbf{1}}(i\not{D}_{\mathbf{1}} - M_S)\Psi_{\mathbf{1}} \\ & + \bar{\tilde{\Psi}}_{\mathbf{7}}(i\not{\nabla} - \tilde{M}_\Psi)\tilde{\Psi}_{\mathbf{7}} + \bar{\tilde{\Psi}}_{\mathbf{1}}(i\not{\partial} - \tilde{M}_S)\tilde{\Psi}_{\mathbf{1}} \\ & + (ic_L\bar{\Psi}^i_{\mathbf{7}L}\not{d}_i\Psi_{\mathbf{1}L} + ic_R\bar{\Psi}^i_{\mathbf{7}R}\not{d}_i\Psi_{\mathbf{1}R} + i\tilde{c}_L\bar{\tilde{\Psi}}^i_{\mathbf{7}L}\not{d}_i\tilde{\Psi}_{\mathbf{1}L} \\ & + i\tilde{c}_R\bar{\tilde{\Psi}}^i_{\mathbf{7}R}\not{d}_i\tilde{\Psi}_{\mathbf{1}R} + \mathrm{H.c.}),\end{aligned} \tag{3.9}$$

where $D_{\mathbf{7}\mu} = \nabla_\mu + iXB_\mu$, $D_{\mathbf{1}\mu} = \partial_\mu + iXB_\mu$, and $\nabla_\mu = \partial_\mu + iE_\mu$. We have introduced two sets of $O(1)$ coefficients, c_L and c_R and their twins, for the interactions mediated by the d_μ operator. Considering the elementary part of the Lagrangian, it comprises just the kinetic terms for the doublets and right-handed tops:

$$\mathcal{L}^F_{\rm elem} = \bar{q}_L i\not{D}q_L + \bar{t}_R i\not{D}t_R + \bar{\tilde{q}}_L i\not{D}\tilde{q}_L + \bar{\tilde{t}}_R i\not{\partial}\tilde{t}_R. \tag{3.10}$$

The final term in our classification is the elementary/composite mixing that we write again following the prescription of partial compositeness. With our choice of quantum numbers for the composite operators, the spurions in Eq. (3.2) can be matched to dimensionless couplings according to

$$\Delta_{\alpha A} = \begin{pmatrix} 0 & 0 & iy_L & -y_L & 0\times 4 \\ iy_L & y_L & 0 & 0 & 0\times 4 \end{pmatrix}, \qquad \Theta_A = y_R, \tag{3.11}$$

and

$$\tilde{\Delta}_{\alpha A} = \begin{pmatrix} 0\times 4 & 0 & 0 & i\tilde{y}_L & -\tilde{y}_L \\ 0\times 4 & i\tilde{y}_L & \tilde{y}_L & 0 & 0 \end{pmatrix}, \qquad \tilde{\Theta}_A = \tilde{y}_R, \tag{3.12}$$

[5]Notice that in the Lagrangian (3.7), the parameters f, M_ρ, M_{ρ^X}, g_ρ, and g_{ρ^X} are all independent. It is common to define the parameters $a_\rho = M_\rho/(g_\rho f)$ and $a_{\rho^X} = M_{\rho^X}/(g_{\rho^X} f)$, which are expected to be $O(1)$. In our analysis we set $a_\rho = 1/\sqrt{2}$ corresponding to the two-site model value (see the last paragraph of this section) and $a_{\rho^X} = 1$.

[6]Notice that in general we should introduce two different singlets in our Lagrangian. One corresponds to a full $SO(8)$ singlet, while the other is the $SO(7)$ singlet appearing in the decomposition $\mathbf{8} = \mathbf{7} + \mathbf{1}$ of the fundamental of $SO(8)$ under the $SO(7)$ subgroup. We will further simplify our study identifying the two singlets with just one composite particle.

where we have introduced the elementary/composite mixing parameters y_L, y_R and their twin counterparts. These dimensionless y's control the strength of the interaction between the elementary and composite resonance fields, according to the Lagrangian:

$$\mathcal{L}^F_{\rm mix} = f(\bar{q}^\alpha_L \Delta_{\alpha A}\Sigma_{Ai}\Psi^i_{\mathbf{7}} + \bar{q}^\alpha_L \Delta_{\alpha A}\Sigma_{A8}\Psi_{\mathbf{1}} + y_R \bar{t}_R \Psi_{\mathbf{1}} + \text{H.c.}) + f(\bar{\tilde{q}}^\alpha_L \tilde{\Delta}_{\alpha A}\Sigma_{Ai}\tilde{\Psi}^i_{\mathbf{7}} + \bar{\tilde{q}}^\alpha_L \tilde{\Delta}_{\alpha A}\Sigma_{A8}\tilde{\Psi}_{\mathbf{1}} + \tilde{y}_R \bar{\tilde{t}}_R \tilde{\Psi}_{\mathbf{1}} + \text{H.c.}). \tag{3.13}$$

Depending on the UV boundary condition and the relevance or marginality of the operators appearing in Eq. (3.2), the y's can vary from weak to $O(g_*)$. Correspondingly the light fermions vary from being completely elementary (for y weak) to effectively fully composite (for $y \sim g_*$). For reasons that will become clear, given $y_t \sim y_L y_R/g_*$, it is convenient to take $y_L \simeq \tilde{y}_L \sim y_t$, i.e., weak left mixing, and $y_R \simeq \tilde{y}_R \sim g_*$. For such strong right-handed mixing the right-handed tops can be practically considered part of the strong sector.

The last term that we need to introduce in the effective Lagrangian describes the interactions between the vector and fermion resonances and originates completely in the composite sector. We have:

$$\mathcal{L}^{VF}_{\rm comp} = \sum_{i=L,R} [\alpha_i \bar{\Psi}_{\mathbf{7}i}(\not{\partial} - \not{E})\Psi_{\mathbf{7}i} + \alpha_{\mathbf{7}i}\bar{\Psi}_{\mathbf{7}i}(\not{\partial}^X - \not{B})\Psi_{\mathbf{7}i} + \alpha_{\mathbf{1}i}\bar{\Psi}_{\mathbf{1}i}(\not{\partial}^X - \not{B})\Psi_{\mathbf{1}i} + \tilde{\alpha}_i \bar{\tilde{\Psi}}_{\mathbf{7}i}(\not{\partial} - \not{E})\tilde{\Psi}_{\mathbf{7}i} + \tilde{\alpha}_{\mathbf{7}i}\bar{\tilde{\Psi}}_{\mathbf{7}i}(\not{\partial}^X - \not{B})\tilde{\Psi}_{\mathbf{7}i} + \tilde{\alpha}_{\mathbf{1}i}\bar{\tilde{\Psi}}_{\mathbf{1}i}(\not{\partial}^X - \not{B})\tilde{\Psi}_{\mathbf{1}i}], \tag{3.14}$$

where all the coefficients α_i appearing in the Lagrangian are $O(1)$ parameters.

We conclude the discussion of our effective Lagrangian by clarifying its two-site model limit [44] (see also Ref. [45]). This is obtained by combining the singlet and the septuplet into a complete representation of $SO(8)$, so that the model enjoys an enhanced $SO(8)_L \times SO(8)_R$ global symmetry. This is achieved by setting $c_L = c_R = \tilde{c}_L = \tilde{c}_R = 0$ and all the α_i equal to 1. Moreover, we have to impose $M_\rho = g_\rho f/\sqrt{2}$, so that the heavy vector resonances can be reinterpreted as gauge fields of $SO(7)$. As shown in Ref. [44], with this choice of the free parameters the Higgs potential becomes calculable up to only a logarithmic divergence, that one can regulate by imposing just one renormalization condition. In the subsequent sections, we will extensively analyze the EW precision constraints in the general case, as well as in the two-site limit.

B. Perturbativity of the simplified model

In Sec. II A 1 it was noted that a TH construction typically involves large multiplicities of states and, as a consequence, the dynamics responsible for its UV completion cannot be maximally strongly coupled. This in turn limits the improvement in fine tuning that can be achieved compared to standard scenarios of EWSB. In our naive estimates of Eqs. (2.3), (2.7), and (2.9) the interaction strength of the UV theory was controlled by the σ-model quartic coupling $\lambda_{\mathcal{H}}$ or, equivalently, by m_σ/f. By considering the $\lambda_{\mathcal{H}}$ one-loop β-function [Eq. (2.5)] we estimated the maximal value of $\lambda_{\mathcal{H}}$ as the one corresponding to an $O(1)$ relative change through one e-folding of RG evolution. For an $SO(8)/SO(7)$ σ-model this led to $\sqrt{\lambda_{\mathcal{H}}} \lesssim \sqrt{2}\pi$, or, equivalently, $m_\sigma/f \lesssim \pi$.

Alternatively, the limit set by perturbativity on the UV interaction strength may also be estimated in the effective theory described by the nonlinear σ-model by determining the energy scale at which tree-level scattering amplitudes become nonperturbative. For concreteness, we considered the following two types of scattering processes: $\pi\pi \to \pi\pi$ and $\pi\pi \to \bar{\psi}\psi$, where π are the NGBs and $\psi = \{\Psi_7, \tilde{\Psi}_7\}$ denotes a composite fermion transforming in the fundamental of $SO(7)$. Other processes can (and should) be considered, with the actual bound being given by the strongest of the constraints obtained in this way.

Requiring that the process $\pi\pi \to \pi\pi$ stay perturbative up the cutoff scale m_* gives the bound

$$\frac{M_\rho}{f} \sim \frac{M_\Psi}{f} \lesssim \frac{m_*}{f} < \frac{4\pi}{\sqrt{N-2}} \simeq 5.1, \tag{3.15}$$

where the second inequality is valid in a generic $SO(N)/SO(N-1)$ nonlinear σ-model, and we have set $N = 8$ in the last step. More details on how this result was obtained can be found in Appendix G. Equation (3.15) in fact corresponds to a limit on the interaction strength of the UV theory, given that the couplings among fermion and vector resonances are of order M_Ψ/f and M_ρ/f, respectively. Perturbativity of the scattering amplitude for $\pi\pi \to \bar{\psi}\psi$ instead gives (see Appendix G for details)

$$\frac{M_\rho}{f} \sim \frac{M_\Psi}{f} \lesssim \frac{m_*}{f} < \frac{\sqrt{12\sqrt{2}}\pi}{\sqrt{N_f}} \simeq \frac{4\pi}{\sqrt{N_f}}, \tag{3.16}$$

where N_f is the multiplicity of composite fermions (including the number of colors and families). Our simplified model with one family of composite fermions has $N_f = 6$, which gives a limit similar to Eq. (3.15):

$M_\Psi/f \lesssim 5.3$. A model with three families of composite quarks and leptons has instead $N_f = 24$, from which follows the stronger bound $M_\Psi/f \lesssim 2.6$.

As a third alternative, one could analyze when 1-loop corrections to a given observable become of the same order as its tree-level value. We applied this criterion to our simplified model by considering the $\hat{S}$ parameter, the new physics contribution to which includes a tree-level correction from heavy vectors given by Eq. (5.6), and a one-loop correction due to heavy fermions, which can be found in Appendix E. By requiring that the one-loop term be smaller than the tree-level correction, we obtain a bound on the strong coupling constant g_ρ. As an illustration, we consider the two-site model limit $c_L = c_R = 0$ and $M_\rho = g_\rho f/\sqrt{2}$ and keep the dominant UV contribution to $\hat{S}$ in Eq. (E7) which is logarithmically sensitive to the cutoff. By setting $m_* = 2M_\Psi$, we find:

$$\frac{\Delta\hat{S}_{1-\text{loop}}}{\Delta\hat{S}_{\text{tree}}} < 1 \Rightarrow \frac{M_\rho}{f} = \frac{g_\rho}{\sqrt{2}} < \frac{\pi}{\sqrt{2\log 2}} \simeq 2.7. \quad (3.17)$$

The perturbative limits obtained from Eqs. (3.15), (3.16), and (3.17) are comparable to that on $\lambda_{\mathcal{H}}$ derived in Sec. II A 1. As already discussed there, one could take any of these results as indicative of the maximal interaction strength in the underlying UV dynamics, though none of them should be considered as a sharp exclusion condition. In our analysis of EW observables we will make use of Eq. (3.15) with $N = 8$ and of Eq. (3.16) with $N_f = 24$ to highlight the regions of parameter space where our perturbative calculation is less reliable. We use both limits as a measure of the intrinsic uncertainty which is inevitably associated with this type of estimation.

IV. HIGGS EFFECTIVE POTENTIAL

As anticipated in the general discussion of Sec. II A, a potential for the Higgs boson is generated at the scale m_* by loops of heavy states through the $SO(8)$-breaking couplings of the elementary fields to the strong sector. Once written in terms of the Higgs boson h (where $H^\dagger H = f^2\sin^2(h/f)/2$, $\tilde{H}^\dagger\tilde{H} = f^2\cos^2(h/f)/2$), at 1-loop this UV threshold contribution has the form [13]:

$$\frac{V(m_*)}{f^4} = \frac{3}{32\pi^2}\left[\frac{1}{16}g_1^2 g_\rho^2 L_1 + (y_L^2 - \tilde{y}_L^2)g_\Psi^2 L_2\right]\sin^2\frac{h}{f} + \frac{3y_L^4}{64\pi^2}F_1\left(\sin^4\frac{h}{f} + \cos^4\frac{h}{f}\right), \quad (4.1)$$

where $g_\Psi \equiv M_\Psi/f$, L_1, L_2, F_1 are $O(1)$ dimensionless functions of the masses and couplings of the theory and the explicit expression of the function F_1 is reported in Eq. (C1) of Appendix C. The first term in the above equation originates from Z_2-breaking effects.[7] The second term, generated by loops of fermions, is Z_2 symmetric and explicitly violates the $SO(8)$ invariance; it thus corresponds to the (UV part of the) last term of Eq. (2.1). Upon electroweak symmetry breaking, Eq. (4.1) contributes to the physical Higgs mass an amount equal to

$$\delta m_h^2|_{\text{UV}} = \frac{3y_L^4}{4\pi^2}F_1 f^2\xi(1-\xi), \quad (4.2)$$

where ξ controls the degree of vacuum misalignment:

$$\xi \equiv \sin^2\frac{\langle h\rangle}{f} = \frac{v^2}{f^2}. \quad (4.3)$$

Below the scale m_* an important contribution to the potential arises from loops of light states, in particular from the top quark and from its twin. The bulk of this IR contribution is captured by the RG evolution of the Higgs potential from the scale m_* down to the electroweak scale. As noted in previous studies (see, e.g., Ref. [13]), for sufficiently large m_* this IR effect dominates over the UV threshold correction and can reproduce the experimental Higgs mass almost entirely. An analogous IR correction to the Higgs quartic arises in SUSY theories with large stop masses, from loops of top quarks. The distinctive feature of any TH scenario, including our model, is the additional twin top contribution.

The Higgs effective action, including the leading $O(\xi)$ corrections associated with operators of dimension 6, was computed at 1-loop in Ref. [13]; the resulting IR contribution to m_h^2 was found to be

$$\delta m_h^2|_{\text{IR}}^{1-\text{loop}} = \frac{3y_t^4}{8\pi^2}f^2\xi(1-\xi)\left(\log\frac{m_*^2}{m_t^2} + \log\frac{m_*^2}{\tilde{m}_t^2}\right), \quad (4.4)$$

where y_t denotes the top Yukawa coupling. The two single-log terms in parentheses correspond to the IR contributions to the effective Higgs quartic λ_h from the top quark and twin top respectively. Leading-logarithmic corrections of the form $(\alpha\log)^n$, arising at higher loops have however an important numerical impact.[8] For example, $(\alpha\log)^2$ corrections generated by 2-loop diagrams (mostly due to the running of the top and twin top Yukawa couplings, that are induced by respectively QCD and twin QCD) are expected to give a $\sim$30% reduction in the Higgs mass for $m_* \simeq 5$ TeV.

We have computed the IR contribution to the Higgs mass in a combined expansion in ξ and $(\alpha\log)$. We have included the LO electroweak contribution, all terms up to NLO in α_t

[7]Subleading Z_2-breaking terms have been neglected for simplicity. The complete expressions are given in Ref. [13].

[8]Here $\alpha = g_{\text{SM}}^2/4\pi$, with g_{SM} being any large SM coupling, i.e., g_S and y_t.

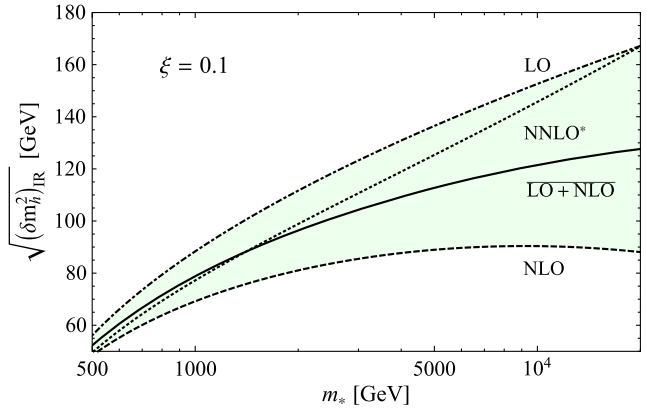

FIG. 1. IR contribution to the Higgs mass as a function of the scale m_* for $\xi = 0.1$. The dot-dashed (upper) and dashed (lower) curves denote the LO and NLO result in a combined perturbative expansion in $(\alpha \log)$ and ξ. The dotted curve contains the pure QCD part of the NNLO correction (see Appendix C for details). The shaded region represents the uncertainty in our estimate. The central value of this band, given by the solid black line and computed as the average of the LO and NLO results, is the value that we use as our numerical estimate throughout the paper.

and α_S, and some contributions, expected to be leading for not too large m_*, at NNLO in α_S. We report the details in Appendix C.

The value of $(\delta m_h^2|_{\rm IR})^{1/2}$ is shown in Fig. 1 as a function of m_* for $\xi = 0.1$. The upper and lower curves represent respectively the LO and NLO calculation in our combined $(\xi, \alpha \log)$ expansion. Numerically, the naive expectation is confirmed, as the NLO correction decreases $(\delta m_h^2|_{\rm IR})^{1/2}$ by $\sim$35% for $m_* = 5$ TeV. The dotted curve, indicated as NNLO*, includes NNLO contributions of order $\alpha_t \xi^2 \log$, $\alpha_t \alpha_S \xi \log^2$, and $\alpha_t \alpha_S^2 \log^3$ (see Appendix C). Additional contributions of order $\alpha_t^2 \xi \log^2$, $\alpha_t^2 \alpha_S \log^3$ and $\alpha_t^3 \log^3$ are not included. An attempt to include these contributions has been made in Ref. [46]. However, the calculation presented there misses some additional contributions from the twin GB and does not represent the full NNLO calculation. The picture that we get from our NNLO* calculation and the incomplete result of Ref. [46], is that the NNLO* gives an overestimate of the IR contribution to the Higgs mass as the aforementioned neglected effects are expected to give a reduction. Given the lack of a complete NNLO calculation, we estimate our uncertainty on the IR Higgs mass as the green shaded region lying between the LO and NLO results in Fig. 1. In order to choose, within this uncertainty, a value that is as close as possible to the full NNLO result, in the rest of the paper we take as input value for the IR correction to the Higgs mass the average of the LO and NLO results, corresponding to the solid black line in the figure.

The plot of Fig. 1 illustrates one of the characteristic features of TH models: the IR contribution to the Higgs mass largely accounts for its experimental value and is completely predicted by the theory in terms of the low-energy particle content (SM plus twin states). In particular, considering the aforementioned input value and choosing as a benchmark values $m_* = 5$ TeV and $\xi = 0.1$, we find that the contributions of the SM and twin light degrees of freedom account for around 50% and 40% of the Higgs mass squared, respectively, so that almost the entire experimental value of the Higgs mass can be due only to the IR degrees of freedom. Threshold effects arising at the UV matching scale, on the other hand, are model dependent but give a subleading correction. An accurate prediction of the Higgs mass and an assessment of the plausibility of the model thus requires a precise determination of its IR contribution. Indeed the difference between the IR contribution of Fig. 1 and the measured value $m_h = 125$ GeV must be accounted for by the UV threshold contribution in Eq. (4.2); for our previous benchmark choice of m_*, about 12% of the Higgs mass should be generated by the UV physics. This translates into a generic constraint on the size of y_L, a parameter upon which electroweak precision observables (EWPO) crucially depend, thus creating a nontrivial correlation between the Higgs mass, EWPO and naturalness.

V. ELECTROWEAK PRECISION OBSERVABLES

In this section we compute the contribution of the new states described by our simplified model to the EWPO. Although it neglects the effects of the heavier resonances, our calculation is expected to give a fair assessment of the size of the corrections due to the full strong dynamics, and in particular to reproduce the correlations among different observables.

It is well known that, under the assumption of quark and lepton universality, short-distance corrections to the electroweak observables due to heavy new physics can be expressed in terms of four parameters, $\hat{S}$, $\hat{T}$, W, Y, defined in Ref. [47] (see also Ref. [48] for an equivalent analysis) as a generalization of the parametrization introduced by Peskin and Takeuchi in Refs. [49,50]. Two additional parameters, δg_{Lb} and δg_{Rb}, can be added to account for the modified couplings of the Z boson to left- and right-handed bottom quarks respectively.[9] A naive estimate shows that in CH theories, including our TH model, W and Y are subdominant in an expansion in the weak couplings [31] and can thus be neglected. The small coupling of the right-handed bottom quark to the strong

[9]We define δg_{Lb} and δg_{Rb} in terms of the following effective Lagrangian in the unitary gauge:

$$\mathcal{L}_{\rm eff} \supset \frac{g_2}{2c_W} Z_\mu \bar{b} \gamma^\mu [(g_{Lb}^{\rm SM} + \delta g_{Lb})(1 - \gamma_5) + (g_{Rb}^{\rm SM} + \delta g_{Rb})(1 + \gamma_5)] b + \cdots \quad (5.1)$$

where the dots stand for higher-derivative terms and $g_{Lb}^{\rm SM} = -1/2 + s_W^2/3$, $g_{Rb}^{\rm SM} = s_W^2/3$.

dynamics makes also δg_{Rb} small and negligible in our model. We thus focus on $\hat{S}$, $\hat{T}$, and δg_{Lb}, and compute them by including effects from the exchange of vector and fermion resonances, and from Higgs compositeness.

We work at the 1-loop level and at leading order in the electroweak couplings and perform an expansion in inverse powers of the new physics scale. In this limit, the twin states do not affect the EWPO as a consequence of their being neutral under the SM gauge group. Deviations from the SM predictions arise only from heavy states with SM quantum numbers and are parametrically the same as in ordinary CH models with singlet t_R. This can be easily shown by means of naive dimensional analysis and symmetries as follows. Twin tops interact with the SM fields only through higher-dimensional operators. The operators relevant for the EWPO are those involving either a SM current or a derivative of the hypercharge field strength:

$$O_{B\tilde{t}} = \frac{g'}{m_W^2}\partial^\mu B_{\mu\nu}\bar{\tilde{t}}\gamma^\nu\tilde{t}, \qquad O_{q\tilde{t}} = \frac{1}{v^2}\bar{q}_L\gamma_\mu q_L\bar{\tilde{t}}\gamma^\mu\tilde{t},$$
$$O_{H\tilde{t}} = \frac{i}{v^2}H^\dagger\overleftrightarrow{D}_\mu H\bar{\tilde{t}}\gamma^\mu\tilde{t}, \tag{5.2}$$

where $\tilde{t}$ indicates either a right- or left-handed twin top.[10] The first two operators of Eq. (5.2) are generated at the scale m_* by the tree-level exchange of the ρ_X. Their coefficients (in a basis with canonical kinetic terms) are respectively of order $(m_W^2/m_*^2)(\tilde{y}/g_*)^2$ and $(y_L^2v^2/m_*^2)\times(\tilde{y}/g_*)^2$, where $\tilde{y}$ equals either $\tilde{y}_L$ or $\tilde{y}_R$ depending on the chirality of $\tilde{t}$. The third operator breaks custodial isospin and the only way it can be generated is via the exchange of weakly coupled elementary fields at loop level. Given that the contribution to EWPO is further suppressed by $\tilde{t}$ loops, the third operator can affect EWPO only at, at least, two loops and is thus clearly negligible. By closing the $\tilde{t}$ loops the first two operators can give rise to effects that are schematically of the form BB, $B\bar{q}q$, or $(\bar{q}q)^2$. The formally quadratically divergent piece of the loop integral renormalizes the corresponding dimension-6 operators. For instance the second structure gives

$$C\frac{g'}{16\pi^2}\frac{y_L^2}{m_*^2}\left(\frac{\tilde{y}}{g_*}\right)^4\partial_\nu B^{\mu\nu}\bar{q}_L\gamma_\mu q_L \tag{5.3}$$

with C an $O(1)$ coefficient which depends on the details of the physics at the scale m_*. Using the equations of motion for B, the above operator gives rise to a correction to the $Zb\bar{b}$ vertex of relative size

$$\frac{\delta g_{Lb}}{g_{Lb}} \sim \frac{g'^2}{16\pi^2}\frac{y_L^2v^2}{m_*^2}\left(\frac{\tilde{y}}{g_*}\right)^4 \tag{5.4}$$

which, even assuming $\tilde{y}\sim g_*$, is $O(g'/y_t)^2$ suppressed with respect to the leading visible sector effect we discuss below. Aside the quadratically divergent piece there is also a logarithmic divergent piece whose overall coefficient is calculable. The result is further suppressed with respect to the above contribution by a factor $(m_t^2/m_*^2)\ln(m_t^2/m_*^2)$.

An additional contribution could in principle come from loops of the extra three "twin" NGBs contained in the coset $SO(8)/SO(7)$. Simple inspection however shows that there is no corresponding 1-loop diagram contributing to the EWPO. In the end we conclude that the effect of twin loops is negligible.

Since the effects from the twin sector can be neglected, the corrections to $\hat{S}$, $\hat{T}$, and δg_{Lb} are parametrically the same as in ordinary CH models. We now give a concise review of the contributions to each of these quantities, distinguishing between the threshold correction generated at the scale m_* and the contribution arising from the RG evolution down to the electroweak scale. For recent analyses of the EWPO in the context of $SO(5)/SO(4)$ CH models see for example Refs. [29,30,45].

A. $\hat{S}$ parameter

The leading contribution to the $\hat{S}$ parameter arises at tree level from the exchange of spin-1 resonances. Since only the (3,1) and (1,3) components of the spin-1 multiplet contribute, its expression is the same as in $SO(5)/SO(4)$ composite-Higgs theories[11]:

$$\Delta\hat{S}_\rho = \frac{g_2^2}{2g_\rho^2}\xi. \tag{5.5}$$

In our numerical analysis presented in Sec. VI we use the two-site model relation $M_\rho = g_\rho f/\sqrt{2}$ to rewrite

$$\Delta\hat{S}_\rho = \frac{m_W^2}{M_\rho^2}. \tag{5.6}$$

The 1-loop contribution from loops of spin-1 and fermion resonances is subdominant (by a factor $g_*^2/16\pi^2$) and will be neglected for simplicity in the following. Nevertheless, we explicitly computed the fermionic contribution (see Appendix E) to monitor the validity of the perturbative expansion and estimate the limit of strong coupling in our model (a discussion on this aspect was given in Sec. III B). An additional threshold correction to $\hat{S}$, naively of the same order as Eq. (5.6), arises from the exchange of cutoff modes

[10]Notice that $O_{H\tilde{t}}$ can be rewritten in terms of the other two operators by using the equations of motion, but it is still useful to consider it in our discussion.

[11]We neglect for simplicity a contribution from the operator $E_{\mu\nu}\rho^{\mu\nu}$, which also arises at tree level. See for example the discussion in Refs. [45,51].

at m_*. As already anticipated, we neglect this correction in the following. In this respect our calculation is subject to an $O(1)$ uncertainty and should rather be considered as an estimate, possibly more refined than a naive one, which takes the correlations among different observables into account.

Besides the UV threshold effects described above, $\hat{S}$ gets an IR contribution from RG evolution down to the electroweak scale. The leading effect of this type comes from the compositeness of the Higgs boson, and is the same as in $SO(5)/SO(4)$ CH models [32]:

$$\Delta\hat{S}_h = \frac{g_2^2}{192\pi^2}\xi \log\frac{m_*^2}{m_h^2}. \tag{5.7}$$

In the effective theory below m_* this corresponds to the evolution of the dimension-6 operators

$$\begin{aligned} O_W &= \frac{ig}{2m_W^2} H^\dagger \sigma^i \overleftrightarrow{D^\mu} H D^\nu W^i_{\mu\nu}, \\ O_B &= \frac{ig'}{2m_W^2} H^\dagger \overleftrightarrow{D^\mu} H \partial^\nu B_{\mu\nu} \end{aligned} \tag{5.8}$$

induced by a 1-loop insertion of

$$O_H = \frac{1}{2v^2}\partial^\mu (H^\dagger H)\partial_\mu (H^\dagger H). \tag{5.9}$$

Denoting with $\bar{c}_i$ the coefficients of the effective operators and working at leading order in the SM couplings, the RG evolution can be expressed as

$$\bar{c}_i(\mu) = \left(\delta_{ij} + \gamma_{ij}\log\frac{\mu}{M}\right)\bar{c}_j(M), \tag{5.10}$$

where γ_{ij} is the anomalous dimension matrix (computed at leading order in the SM couplings). The $\hat{S}$ parameter gets a correction $\Delta\hat{S} = (\bar{c}_W(m_Z) + \bar{c}_B(m_Z))\xi$, and one has $\gamma_{W,H} + \gamma_{B,H} = -g_2^2/(96\pi^2)$. An additional contribution to the running arises from insertions of the current-current operators

$$\begin{aligned} O_{Hq} &= \frac{i}{v^2}\bar{q}_L\gamma^\mu q_L H^\dagger \overleftrightarrow{D_\mu} H, \\ O'_{Hq} &= \frac{i}{v^2}\bar{q}_L\gamma^\mu\sigma^i q_L H^\dagger \sigma^i \overleftrightarrow{D_\mu} H, \\ O_{Ht} &= \frac{i}{v^2}\bar{t}_R\gamma^\mu t_R H^\dagger \overleftrightarrow{D_\mu} H \end{aligned} \tag{5.11}$$

in a loop of top quarks. This is however suppressed by a factor y_L^2/g_*^2 compared to Eq. (5.7) and will be neglected. The suppression arises because the current-current operators are generated at the matching scale with coefficients proportional to y_L^2.

The total correction to the $\hat{S}$ parameter in our model is $\Delta\hat{S} = \Delta\hat{S}_\rho + \Delta\hat{S}_h$, with the two contributions given by Eqs. (5.6) and (5.7).

B. $\hat{T}$ parameter

Tree-level contributions to the $\hat{T}$ parameter are forbidden in our model by the $SO(3)$ custodial symmetry preserved by the strong dynamics, and can only arise via loops involving the elementary states. A non-vanishing effect arises at the 1-loop level corresponding to a violation of custodial isospin by two units. The leading contribution comes from loops of fermions and is proportional to y_L^4, given that the spurionic transformation rule of y_L is that of a doublet, while y_R is a singlet. We find:

$$\Delta\hat{T}_\Psi = a_{\rm UV}N_c\frac{y_L^2}{16\pi^2}\frac{y_L^2 v^2}{M_\Psi^2} + a_{\rm IR}N_c\frac{y_t^2}{16\pi^2}\frac{y_L^2 v^2}{M_\Psi^2}\log\frac{M_1^2}{m_t^2}, \tag{5.12}$$

where $a_{UV,IR}$ are $O(1)$ coefficients whose values are reported in Appendix E and we have defined $M_1 \equiv \sqrt{M_S^2 + y_R^2 f^2}$. The result is finite and does not depend on the cutoff scale m_*. The first term corresponds to the UV threshold correction generated at the scale $\mu = M_1 \sim M_\Psi$. The second term instead encodes the IR running from the threshold scale down to low energy, due to loops of top quarks. In the effective theory below M_1 it corresponds to the RG evolution of the dimension-6 operator

$$O_T = \frac{1}{2v^2}(H^\dagger \overleftrightarrow{D^\mu} H)^2 \tag{5.13}$$

due to insertions of the current-current operators of Eq. (5.11). In particular, $\Delta\hat{T} = \hat{c}_T(m_Z)\xi$ and one has $\gamma_{T,Ht} = -\gamma_{T,Hq} = 3y_t^2/4\pi^2$, $\gamma_{T,Hq'} = 0$. Notice that the size of the second contribution with respect to the first is $O[(y_t/y_L)^2\log(M_1^2/m_t^2)]$: for $y_t \sim y_L$, that is for fully composite t_R, the IR dominated contribution is formally logarithmically enhanced and dominant.

Further contributions to $\hat{T}$ come from loops of spin-1 resonances, the exchange of cutoff modes and Higgs compositeness. The latter is due to the modified couplings of the composite Higgs to vector bosons and reads [32]:

$$\Delta\hat{T}_h = -\frac{3g_1^2}{64\pi^2}\xi\log\frac{m_*^2}{m_h^2}. \tag{5.14}$$

In the effective theory it corresponds to the running of O_T due to the insertion of the operator O_H in a loop with hypercharge. The contribution is of the form of Eq. (5.10) with $\gamma_{T,H} = 3g_1^2/32\pi^2$. The exchange of spin-1 resonances gives a UV threshold correction which is also proportional to g_1^2 (as a spurion, the hypercharge coupling transforms as an isospin triplet), but without any log enhancement. It is

thus subleading compared to Eq. (5.14) and we will neglect it for simplicity (see Ref. [45] for the corresponding computation in the context of $SO(5)/SO(4)$ models). Finally, we also omit the effect of the cutoff modes because it is incalculable, although naively this is of the same order as the contribution from states included in our simplified model. Our result is thus subject to an $O(1)$ uncertainty.

The total contribution to the $\hat{T}$ parameter in our model is therefore $\Delta\hat{T} = \Delta\hat{T}_h + \Delta\hat{T}_\Psi$ with the two contributions given by Eqs. (5.12) and (5.14).

C. δg_{Lb}

In the limit of vanishing transferred momentum, tree-level corrections to δg_{Lb} are forbidden by the P_{LR} parity of the strong dynamics that exchanges $SU(2)_L$ with $SU(2)_R$ in the visible $SO(4)$ and $\widetilde{SU}(2)_L$ with $\widetilde{SU}(2)_R$ in the twin $\widetilde{SO}(4)$ (see Appendix A for details). This is a simple extension of the P_{LR} symmetry of CH models which protects the $Zb\bar{b}$ coupling from large corrections [52]. In our case P_{LR} is an element of the unbroken $SO(7)$ and keeps the vacuum unchanged. It is thus an exact invariance of the strong dynamics, differently from $SO(5)/SO(4)$ models where it is accidental at $O(p^2)$. The gauge couplings $g_{1,2}$ and y_L explicitly break it, while y_R preserves it. At finite external momentum δg_{Lb} gets a non-vanishing tree-level contribution:

$$(\delta g_{Lb})_{\rm tree} = \frac{f^2\xi}{8M_\rho^2}[g_1^2(\alpha_L + \alpha_{\gamma_L}) - g_2^2\alpha_L]\frac{y_L^2 f^2}{M_\Psi^2 + y_L^2 f^2}. \tag{5.15}$$

In the effective theory below M_1, this correction arises from the dimension-6 operators

$$O_{Bq} = \frac{g'}{m_W^2}\partial^\mu B_{\mu\nu}\bar{q}_L\gamma^\nu q_L, \quad O_{Wq} = \frac{g}{m_W^2}D^\mu W^a_{\mu\nu}\bar{q}_L\gamma^\nu\sigma^a q_L,. \tag{5.16}$$

It is of order $(y_L^2/g_*^2)(g^2/g_*^2)\xi$, hence a factor g^2/g_*^2 smaller than the naive expectation in absence of the P_{LR} protection.

At the 1-loop level, corrections to δg_{Lb} arise from the virtual exchange of heavy fermion and vector states. The leading effect comes at $O(y_L^4)$ from loops of heavy fermions (the corresponding diagrams are those of Figs. 4 and 5) and reads

$$(\delta g_{Lb})_\Psi = \frac{y_L^2}{16\pi^2}N_c\frac{y_L^2 v^2}{M_\Psi^2}\left(b_{\rm UV} + c_{\rm UV}\log\frac{m_*^2}{M_\Psi^2}\right) + b_{\rm IR}\frac{y_t^2}{16\pi^2}N_c\frac{y_L^2 v^2}{M_\Psi^2}\log\frac{M_1^2}{m_t^2}. \tag{5.17}$$

The expressions of the $O(1)$ coefficients $b_{UV,IR}$ and $c_{\rm UV}$ are reported in Appendix E. The first term is logarithmically divergent and encodes the UV threshold correction at the matching scale. The divergence comes, in particular, from diagrams where the fermion loop is connected to the b-quark current through the exchange of a spin-1 resonance [29]. A simple operator analysis shows that the threshold contribution from the vector resonances in the adjoint of $SO(7)$ identically vanishes in our model (see Appendix D for details). An additional UV threshold contribution to δg_{Lb} arises from diagrams where the spin-1 resonances circulate in the loop. For simplicity we will not include such effect in our analysis (see Ref. [30] for the corresponding computation in the context of $SO(5)/SO(4)$ models). It is however easy to show that there is no possible diagram with ρ_X circulating in the loop as a consequence of its quantum numbers, while the corresponding contribution from vector resonances in the adjoint of $SO(7)$ is nonvanishing in this case.

The second term in Eq. (5.17) accounts for the IR running down to the electroweak scale. In the effective theory below M_1 one has $\delta g_{Lb} = -(\bar{c}_{Hq}(m_Z) + \bar{c}'_{Hq}(m_Z))/2$, hence the IR correction arises from the evolution of the operators O_{Hq} and O'_{Hq} due to loops of top quarks. In this case the operators that contribute to the running via their 1-loop insertion are those of Eq. (5.11) as well as the following four-quark operators [53]:

$$O_{LR} = (\bar{q}_L\gamma^\mu q_L)(\bar{t}_R\gamma_\mu t_R), \qquad O_{LL} = (\bar{q}_L\gamma^\mu q_L)(\bar{q}_L\gamma_\mu q_L),$$
$$O'_{LL} = (\bar{q}_L\sigma^a\gamma^\mu q_L)(\bar{q}_L\sigma^a\gamma_\mu q_L). \tag{5.18}$$

In fact, the operators contributing at $O(y_L^2 y_t^2)$ to Eq. (5.10) are only those generated at $O(y_L^2)$ at the matching scale; these are O_{Ht}, the linear combination $O_{Hq} - O'_{Hq}$ (even under P_{LR}), and O_{LR} (generated via the exchange of ρ_X).[12] Notice finally that the relative size of the IR and UV contributions to δg_{Lb} is $O[(y_t/y_L)^2\log(M_1^2/m_t^2)]$ precisely like in the case of $\Delta\hat{T}_\Psi$.

It is interesting that in our model the fermionic corrections to δg_{Lb} and $\hat{T}$ are parametrically of the same order and their signs tend to be correlated. It is for example well known that a heavy fermion with the quantum numbers of t_R gives a positive correction to both quantities [28,54–56]. We have verified that this is also the case in our model for $M_S \ll M_\Psi \sim M_\rho$ (light singlet).[13] Conversely, a light septuplet ($M_\Psi \ll M_S \sim M_\rho$) gives a negative contribution to both δg_{Lb} and $\hat{T}$.[14] Although in general the expressions for $\Delta\hat{T}_\Psi$ and $(\delta g_{Lb})_\Psi$ are uncorrelated, their signs tend to be the same whenever the contribution from ρ_X to Eq. (5.17) is

[12]The operators O_{LL} and O'_{LL} are generated at $O(y_L^4)$ by the tree-level exchange of both ρ_X and ρ.

[13]In this limit one has $\Delta\hat{T}_\Psi \simeq 3(\delta g_{Lb})_\Psi$.

[14]The existence of a similar sign correlation in the limit of a light (2,2) has been pointed out in the context of $SO(5)/SO(4)$ CH models, see Ref. [29].

subleading. The sign correlation can instead be broken if ρ_X contributes significantly to δg_{Lb} [in particular, $(\delta g_{Lb})_\Psi$ can be negative for $\alpha_{iL} = -\alpha_{iR}$]. The importance of the above considerations lies in the fact that EW precision data prefer a positive $\hat{T}$ and a negative δg_{Lb}. Situations when both quantities have the same sign are thus experimentally disfavored.

Considering that no additional correction to δg_{Lb} arises from Higgs compositeness, and that we neglect as before the incalculable effect due to cutoff states, the total contribution in our model is $\delta g_{Lb} = (\delta g_{Lb})_{\text{tree}} + (\delta g_{Lb})_\Psi$, with the two contributions given by eqs. (5.15) and (5.17).

VI. RESULTS AND DISCUSSION

We are now ready to translate the prediction for the Higgs mass and the EWPO into bounds on the parameter space of our simplified model and for the composite TH in general. We are interested in quantifying the degree of fine tuning that our construction suffers when requiring the mass scale of the heavy fermions to lie above the ultimate experimental reach of the LHC. As discussed in Sec. II, this scale receives the largest boost from the TH mechanism (without a corresponding increase in the fine tuning of the Higgs mass) in the regime of parameters corresponding to a fully strongly coupled theory, where no quantitatively precise EFT description is allowed. Our computations of physical quantities in this most relevant regime should then be interpreted as an *educated naive dimensional analysis* (eNDA) estimate, where one hopes to capture the generic size of effects beyond the naivest 4π counting, and including factors of a few related to multiplet size, to spin, and to numerical accidents. In the limit where M_ρ/f and M_Ψ/f are significantly below their perturbative upper bounds our computations are well defined. eNDA then corresponds to assuming that the results do not change by more than $O(1)$ (i.e. less than $O(5)$ to be more explicit) when extrapolating to a scenario where the resonance mass scale sits at strong coupling. In practice we shall consider the resonant masses up to their perturbativity bound and vary the α_i and c_i parameters within an $O(1)$ range.[15] In view of the generous parameter space that we shall explore our analysis should be viewed as conservative, in the sense that a realistic TH model will never do better.

Let us now describe the various pieces of our analysis. Consider first the Higgs potential, where the dependence on physics at the resonance mass scale is encapsulated in the function F_1 [Eq. (4.2)] which controls the UV threshold correction to the Higgs quartic. It is calculable in our simplified model and the result is $O(1)$ [its expression is reported in Eq. (C1)], but it can easily be made a bit smaller at the price of some mild tuning by varying the field content or the representations of the heavy fermions. In order to account for these options and thus broaden the scope of our analysis we will treat F_1 as a free $O(1)$ parameter. The value of F_1 has a direct impact on the size of the left-handed top mixing y_L, since $\delta m_h^2|_{\text{UV}} \sim y_L^4 F_1$, and hence controls the interplay between the Higgs potential and EWPO. Specifically, as we already stressed, a smaller F_1 implies a larger value of y_L, which in turn gives a larger $\Delta\hat{T} \propto y_L^4 v^2/M_\Psi^2$. This could help improve the compatibility with EWPT even for large M_Ψ, at the cost of a small additional tuning due to the need for a clever maneuver in the $\hat{S}, \hat{T}$ plane to get back into the ellipse, as well as the fact that F_1 is generically expected to be $O(1)$. In the following we will thus treat F_1 as an input parameter and use Eqs. (4.2) and (B4) to fix y_L and y_R in terms of the Higgs and top quark experimental masses. Our final results will be shown for two different choices of F_1, namely $F_1 = 1$ and $F_1 = 0.3$, in order to illustrate how the bounds are affected by changing the size of the UV threshold correction to the Higgs potential.

The EWPO and the Higgs mass computed in the previous sections depend on several parameters, in particular on the mass spectrum of resonances (see Appendix B), the parameters c_i, α_i of Eqs. (3.9), (3.14), and the parameter F_1 discussed above. In order to focus on the situation where resonances can escape detection at the LHC, we will assume that their masses are all comparable and that they lie at or just below the cutoff scale. In order to simplify the numerical analysis we thus set $M_\Psi = M_S = \tilde{M}_\Psi = \tilde{M}_S = M_\rho = M_{\rho^X} = m_*/2$. The factor of two difference between M_Ψ and m_* is chosen to avoid setting all UV logarithms of the form $\log(m_*/M_\Psi)$ to zero, while not making them artificially large. As a further simplification we set $c_L = c_R \equiv c$, $\alpha_{\mathbf{7}L} = \alpha_{\mathbf{1}L}$, and $\alpha_{\mathbf{7}R} = \alpha_{\mathbf{1}R}$. The parameter α_L appears only in the tree-level contribution to δg_{Lb}, see Eq. (5.15), and we fix it equal to 1 for simplicity. Even though the above choices represent a significant reduction of the whole available parameter space, for the purpose of our analysis they represent a sufficiently rich set where EWPT can be successfully passed.

Let us now discuss the numerical bounds on the parameter space of our simplified model. They have been obtained by fixing the top and Higgs masses to their experimental value and performing the numerical fit described in Appendix F. As experimental inputs, we use the PDG values of the top quark pole mass $m_t = 173.21 \pm 0.51 \pm 0.71$ (see last paragraph of Appendix C), and of the Higgs mass, $m_h = 125.09 \pm 0.24$ GeV [57]. Figure 2 shows the results of the fit in the (M_Ψ, ξ) plane for $F_1 = 0.3$ (left panel) and $F_1 = 1$ (right panel). In both panels we have set $c = 0$, which corresponds to the two-site model limit of our simplified Lagrangian. The yellow regions correspond to the points that pass the χ^2 test at

[15] Notice indeed that $(\alpha = 1, c = 0)$ and $(\alpha = 0, c = 1/\sqrt{2})$ correspond to specific limits at weak coupling, namely the two-site model and the linear sigma model respectively. This suggests that their natural range is $O(1)$.

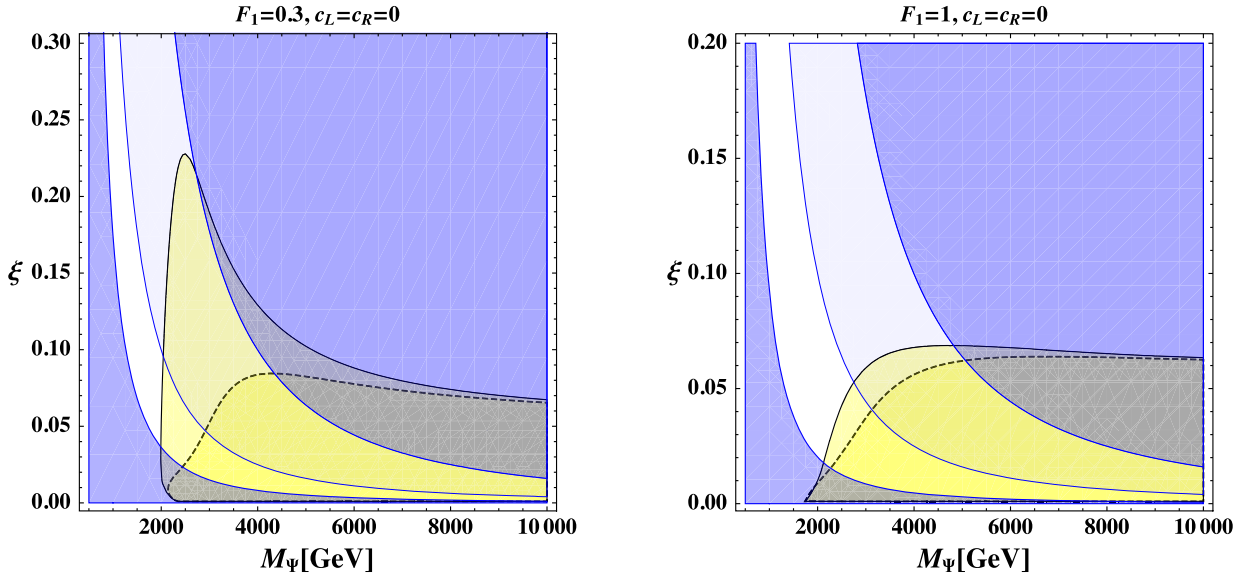

FIG. 2. Allowed regions in the (M_Ψ, ξ) plane for $F_1 = 0.3$ (left panel) and $F_1 = 1$ (right panel). See the text for an explanation of the different regions and of the choice of parameters.

95% confidence level (CL), see Appendix F for details. Solid black contours denote the regions for which $\alpha_{\mathbf{1}L} = -\alpha_{\mathbf{1}R} = 1$, while dashed contours surround the regions obtained with $\alpha_{\mathbf{1}L} = \alpha_{\mathbf{1}R} = 1$. The areas in blue are theoretically inaccessible. The lower left region in dark blue, in particular, corresponds to $M_\Psi/f \equiv g_\Psi < y_L$. The upper dark- and light-blue regions correspond instead to points violating the perturbative limits on g_Ψ given by Eq. (3.15) with $N = 8$, and Eq. (3.16) with $N_f = 24$, respectively (see Sec. III B for a discussion). The difference between these two regions can be taken as an indication of the uncertainty associated with the perturbative bound.[16]

In the left panel of Fig. 2 the allowed (lighter yellow) region extends up to $\xi \simeq 0.2$ for masses M_Ψ in the 2–3 TeV range. Such large values of ξ are possible in this case because the fermionic contribution to $\Delta\hat{T}_\Psi$ turns out to be sufficiently large and positive to compensate for both the negative $\Delta\hat{T}_h$ in Eq. (5.14) and the positive $\Delta\hat{S}_\rho$ and $\Delta\hat{S}_h$ in Eqs. (5.6), (5.7). For larger M_Ψ the fermionic contribution $\Delta\hat{T}_\Psi$ becomes too small and this compensation no longer occurs. In this case, however, the strongest bound comes from the perturbativity limit (blue region), which makes points with large M_Ψ at fixed ξ theoretically inaccessible. Notice that large values of ξ become excluded if one considers the choice $\alpha_{\mathbf{1}L} = \alpha_{\mathbf{1}R} = 1$ leading to the dashed contour. The large difference between the solid and dashed curves (i.e. lighter and darker yellow regions) depends on the sign correlation between $\Delta\hat{T}_\Psi$ and δg_{Lb}. In the case of the solid line, the signs are anticorrelated (e.g., positive $\Delta\hat{T}_\Psi$ and negative δg_{Lb}), allowing for the compensation effect by $\Delta\hat{T}_\Psi$. In the case of the dashed line, instead, the signs of the two parameters are correlated (both positive), so that when $\Delta\hat{T}_\Psi$ is large, δg_{Lb} is also large and positive. This makes it more difficult to pass the χ^2 test, since data prefer a negative δg_{Lb}.

In the right panel of Fig. 2, obtained with $F_1 = 1$, the allowed yellow region shrinks because the larger value of F_1 implies a smaller y_L hence a smaller $\Delta\hat{T}_\Psi$. In this case the χ^2 test is passed only for $\xi < 0.06$, and the difference between the solid and dashed lines is small since the large and positive $\Delta\hat{S}$ always dominates the fit. Masses M_Ψ larger than ~5 TeV are excluded by the perturbative bound, unless one considers smaller values of ξ.

The results of Fig. 2 can change significantly if the parameter c is allowed to be different from zero. In particular, as one can verify from our formulas in Appendix E, positive values of c increase $\Delta\hat{T}$ and as a result the allowed regions in Fig. 2 shift to the right toward larger values of M_Ψ. In this case the perturbative bound excludes a large portion of the region passing the χ^2 test. The effect of varying c is illustrated in Fig. 3, which shows the 95% CL allowed regions in the plane (c, α) for $F_1 = 0.3$ (left panel) and $F_1 = 1$ (right panel). In both panels we have set $\alpha \equiv \alpha_{\mathbf{1}L} = -\alpha_{\mathbf{1}R}$ (ensuring positive $\Delta\hat{T}_\Psi$ and negative δg_{Lb}). The yellow, orange, and red regions correspond, respectively, to $\xi = 0.05$, $\xi = 0.1$, and $\xi = 0.15$, with the masses of the resonances fixed at their perturbative upper bound $M_\rho = M_\Psi = 4\pi f/\sqrt{N-2}$ (which for $N = 8$ gives ~6/4/3.2 TeV). Note that

[16]Notice that because of our choice $m_* = 2M_\Psi$, the scale m_* lies a factor of 2 above the pertubative cutoff. This is compatible with the semiquantitative nature of our estimates. As we stated previously we insisted in keeping $m_* = 2M_\Psi$ because it implies a more generic contribution to electroweak precision observables.

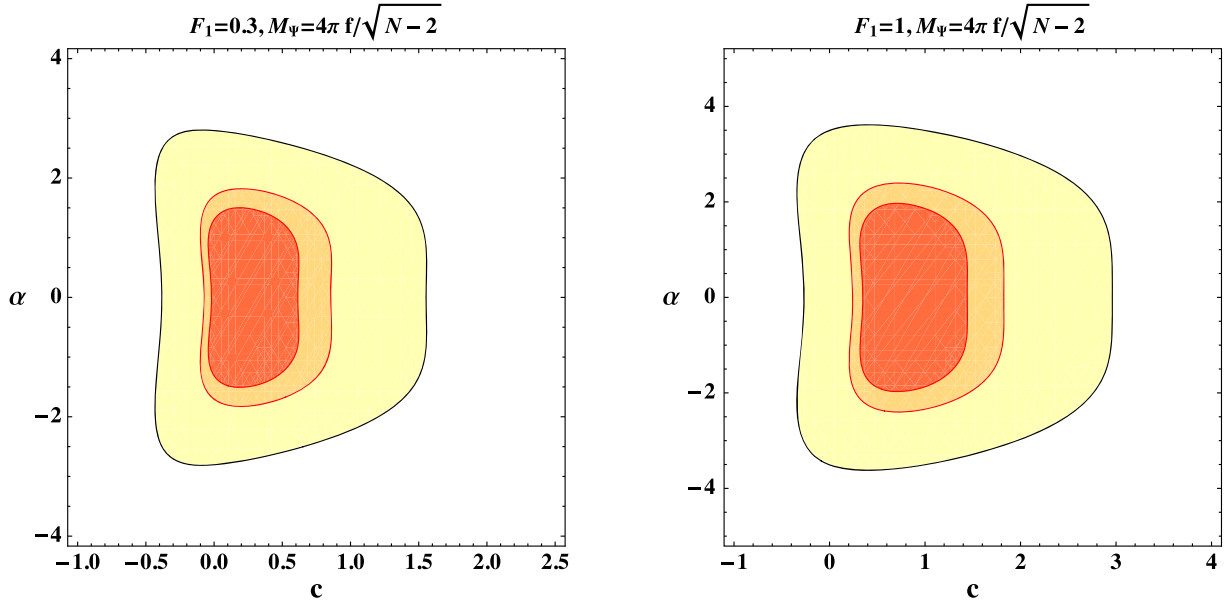

FIG. 3. Allowed regions in the (c, α) plane, with $c = c_L = c_R$, for $F_1 = 0.3$ (left panel) and $F_1 = 1$ (right panel). The yellow, orange, and red regions correspond to $\xi = 0.05$, 0.1 and 0.15 respectively. See the text for an explanation of the choice of the other parameters.

increasing F_1 (reducing y_L) shifts the allowed region toward positive values of c, since as mentioned above, smaller y_L requires a larger positive c to get a large enough $\Delta\hat{T}_\Psi$. Obviously, larger values of ξ correspond to smaller allowed regions, as is clear from Fig. 2. Finally, notice that the vertically symmetric structure of the allowed regions is due to the quadratic dependence of δg_{Lb} on α. From these plots, one can see that for resonances conceivably out of direct reach of the LHC and for $\xi \sim 0.1$, corresponding to about 20% tuning of the Higgs mass, both α and c are allowed to span a good fraction of their expected $O(1)$ range. No dramatic extra tuning in these parameters seems therefore necessary to meet the constraints of EWPT. In particular, considering the plot for $F_1 = 1$ (right panel), one notices that the bulk of the allowed region is at positive c. For instance by choosing $c \sim 0.2$–0.5 the plot in the (ξ, M_Ψ) plane for $F_1 = 1$ becomes quite similar to the one at the left of Fig. 3 valid for $F_1 = 0.3$: there exists a "peak" centered at $M_\Psi \sim 2$–4 TeV and extending up to $\xi \sim 0.2$. The specific choice $c = 0$ is thus particularly restrictive for $F_1 = 1$ (right panel of Fig. 2), but this restriction is lifted for positive c. Overall we conclude that for $\xi \sim 0.1$ and for resonances just beyond the LHC reach, the correct value of the Higgs quartic can be obtained and EWPT passed with only a mild additional tuning associated with a sign correlation $\alpha_{1L} = -\alpha_{1R}$, and a correlation between c and F_1 (e.g. $c > 0$ for $F_1 = 1$). These correlations allow the various contributions to $\hat{T}$ and δg_{Lb} to compensate for each other, achieving agreement with EWPT. If forced to quantify the tuning inherent in these effects, we could estimate it to be around $1/4 = (1/2) \times (1/2)$, given about $1/2$ of the plausible choices for both α_i and c_i are allowed.

VII. SUMMARY

In this paper we tried to assess how plausible a scenario yielding no new particles at the LHC can be obtained using the TH construction. We distinguished three possible classes of models: the subhypersoft, the hypersoft and the superhypersoft, with increasing degree of technical complexity and decreasing (technical) fine tuning. We then focused on the CH incarnation of the simplest option, the subhypersoft scenario, where the boost factor for the mass of colored partners [Eq. (2.4)] at fixed tuning is roughly given by

$$\frac{g_*}{\sqrt{2}y_t} \times \frac{1}{\sqrt{\ln(m_*/m_t)}}. \tag{7.1}$$

Here the gain derives entirely from the relative coupling strength $g_*/\sqrt{2}y_t$, making the marriage of twinning and compositeness practically obligatory. We attempted a more precise estimate of the upper limit on $g_*/\sqrt{2}y_t$, as compared with previous studies (e.g. Ref. [13]). We found by independent but consistent estimates, that the bound ranges from ~3 in a toy sigma model [Eq. (2.6)] to ~5 in a simplified CH model [Eq. (3.15)], with both limits somewhat below the NDA estimate of $4\pi \sim 12$. Consequently for a mild tuning $\epsilon \sim 0.1$ the upper bound on the mass of the resonances with SM quantum numbers is closer to the 3–5 TeV range than it is to 10 TeV. This gain, despite

being less spectacular than naively expected, is still sufficient to push these states out of direct reach of the LHC, provided we resort to full strong coupling. In practice this implies no real computational advantage from considering holographic realizations of composite TH constructions: since the boost factor is controlled by the KK coupling, the 5D description breaks down in precisely the most interesting regime, where the KK coupling is strong. In this situation computations based on an explicit 5D construction, such as the ones studied in Refs. [9,16] for instance, are no better than numerical estimates made in our simplified model. Indeed we have checked that EWPT can be satisfied in a sizable portion of the parameter space, given some interplay among the various contributions. In particular the IR corrections to $\hat{T}$ and $\hat{S}$ are enhanced by $\ln(m_*/m_h)$, and for $\xi > 0.1$ the compensating contribution to $\hat{T}$, which decreases like $1/m_*^2$, is necessary. Given that perturbativity limits m_* to be below 5 TeV for $\xi > 0.1$ (see the upper blue exclusion region in Fig. 2) this compensation in EWPT can still take place at the price of a moderate extra tuning. For ξ of order a few percent on the other hand, EWPT would be passed without any additional tuning, while the masses of SM-charged resonances would be pushed up to the 10 TeV range, where nothing less than a 100 TeV collider would be required to discover them, and that barely so [58,59].

Although EWPT work similarly in the CH and composite TH frameworks, the two are crucially different when it comes to contributions to the Higgs quartic. In the CH these are enhanced when g_*, i.e. m_*/f, is strong and, as discussed for instance in Ref. [33], in order to avoid additional tuning of the Higgs quartic g_* cannot be too large. According to the study in Refs. [60–63] the corresponding upper bound on the mass of the colored top partners in CH reads roughly $m_*/f \lesssim 1.5$; this should be compared to the upper bound $m_*/f \lesssim 5$ from strong coupling we found in Eq. (3.15). The Higgs quartic protection afforded by the TH mechanism allows us to take m_*/f as large as possible, allowing the colored partners to be heavier at fixed f, hence at fixed fine tuning ξ. In the end the gain is about a factor of $5/1.5 \sim 3$, not impressive, but sufficient to place the colored partners outside of LHC reach for a mild tuning $\xi \sim 0.1$.

Finally, we comment on the classes of models not covered in this paper: the hypersoft and superhypersoft scenarios. The latter requires combining supersymmetry and compositeness with the TH mechanism, which, while logically possible, does not correspond to any existing construction. Such a construction would need to be rather ingenious, and we currently do not feel compelled to provide it, given the already rather epicyclic nature of the TH scenario. The simpler hypersoft scenario, though also clever, can by contrast be implemented in a straightforward manner, via, e.g., a tumbling $SO(9) \to SO(8) \to SO(7)$ pattern of symmetry breaking. The advantage of this approach is that it allows us to remain within the weakly-coupled domain, due to the presence of a relatively light twin Higgs scalar mode σ, whose mass can be parametrically close to that of the twin tops, $\sim y_t f$ (around 1 TeV for $\xi \sim 0.1$). As well as giving rise to distinctive experimental signatures due to mixing with the SM Higgs [64], the mass of the light σ acts as a UV cutoff for the IR contributions to $\hat{S}$ and $\hat{T}$ in Eqs. (5.7) and (5.14) [12]. For sufficiently light σ then, less or no interplay between the various contributions is required in order to pass EWPT. Together with calculability, this property may well single out the hypersoft scenario as the most plausible TH construction.

ACKNOWLEDGMENTS

We would like to thank Andrey Katz, Alberto Mariotti, Kin Mimouni, Giuliano Panico, Diego Redigolo, Matteo Salvarezza, and Andrea Wulzer for useful discussions. The Swiss National Science Foundation partially supported the work of D. G. and R. R. under Contracts No. 200020-150060 and No. 200020-169696, the work of R. C. under Contract No. 200021-160190, and the work of R. T. under the Sinergia network CRSII2-160814. The work of R. C. was partly supported by the ERC Advanced Grant No. 267985 *Electroweak Symmetry Breaking, Flavour and Dark Matter: One Solution for Three Mysteries (DaMeSyFla)*. R. M. is supported by ERC Grant No. 614577 HICCUP High Impact Cross Section Calculations for Ultimate Precision.

APPENDIX A: $SO(8)$ GENERATORS AND CCWZ VARIABLES

In this Appendix we define the generators of the $SO(8)$ algebra and describe the $SO(8)/SO(7)$ symmetry-breaking pattern, introducing the CCWZ variables for our model. We refer the reader to Refs. [41,42] for a detailed analysis of this procedure and we closely follow the notation of Ref. [13].

We start by listing the twenty-eight generators of $SO(8)$ and decomposing them into irreducible representations of the unbroken subgroup $SO(7)$: $\mathbf{28} = \mathbf{7} \oplus \mathbf{21}$. They can be compactly written as:

$$(T_{ij})_{kl} = \frac{i}{\sqrt{2}}(\delta_{ik}\delta_{jl} - \delta_{il}\delta_{jk}), \tag{A1}$$

with $i, j, k, l = 1, \ldots, 8$. We choose to align the vacuum expectation value responsible for the spontaneous breaking of $SO(8)$ to $SO(7)$ along the 8th component: $\phi_0 = f(0, 0, 0, 0, 0, 0, 0, 1)^t$. With this choice, the broken and unbroken generators, transforming, respectively, in the **7** and **21** of $SO(7)$, are

$$(T^{\mathbf{7}}_{\beta})_{\gamma\rho} = \frac{i}{\sqrt{2}}(\delta_{8\gamma}\delta_{\beta\rho} - \delta_{8\rho}\delta_{\beta\gamma}),$$
$$(T^{\mathbf{21}}_{\alpha\beta})_{\gamma\rho} = \frac{i}{\sqrt{2}}(\delta_{\alpha\gamma}\delta_{\beta\rho} - \delta_{\alpha\rho}\delta_{\beta\gamma}), \tag{A2}$$

where $\alpha,\beta = 1,\ldots,7$ and $\gamma,\rho = 1,\ldots,8$. It is useful to identify the subgroups $SO(4) \sim SU(2)_L \times SU(2)_R$ and $\widetilde{SO}(4) \sim \widetilde{SU}(2)_L \times \widetilde{SU}(2)_R$ of $SO(8)$; they are generated by:

$$(T_{\mathbf{L}})^{\alpha} = \begin{pmatrix} t^{\alpha}_{\mathbf{L}} & 0 \\ 0 & 0 \end{pmatrix}, \qquad (T_{\mathbf{R}})^{\alpha} = \begin{pmatrix} t^{\alpha}_{\mathbf{R}} & 0 \\ 0 & 0 \end{pmatrix},$$
$$(\tilde{T}_{\mathbf{L}})^{\alpha} = \begin{pmatrix} 0 & 0 \\ 0 & t^{\alpha}_{\mathbf{L}} \end{pmatrix}, \qquad (\tilde{T}_{\mathbf{R}})^{\alpha} = \begin{pmatrix} 0 & 0 \\ 0 & t^{\alpha}_{\mathbf{R}} \end{pmatrix}, \tag{A3}$$

where $t^{\alpha}_{\mathbf{L}}$ and $t^{\alpha}_{\mathbf{R}}$ are 4×4 matrices defined as

$$(t^{\alpha}_{\mathbf{L},\mathbf{R}})_{ij} = -\frac{i}{2}\left[\frac{1}{2}\epsilon^{\alpha\beta\gamma}(\delta^{\beta}_{i}\delta^{\gamma}_{j} - \delta^{\beta}_{j}\delta^{\gamma}_{i}) \pm (\delta^{\alpha}_{i}\delta^{4}_{j} - \delta^{\alpha}_{j}\delta^{4}_{i})\right] \tag{A4}$$

with $\alpha = 1,2,3$ and $i,j = 1,\ldots,4$. The elementary SM and twin vector bosons gauge, respectively, a subgroup $SU(2)_L \times U(1)_Y$ of $SO(4)$, with $U(1)_Y \equiv U(1)_{R3}$, and the subgroup $\widetilde{SU}(2)_L$ inside $\widetilde{SO}(4)$. This choice corresponds to having zero vacuum misalignment at tree level.

The spontaneous breaking of $SO(8)$ to $SO(7)$ delivers seven NGBs, that we collect in the vector $\mathbf{\Pi} = (\pi_2, \pi_1, -\pi_3, \pi_4, \tilde{\pi}_2, \tilde{\pi}_1, -\tilde{\pi}_3)^t$. The first four transform as a fundamental of $SO(4)$ and form the Higgs doublet; the remaining three are singlets of $SO(4)$ and are thus neutral under the SM gauge group. All together they can be arranged in the Goldstone matrix

$$\Sigma(\mathbf{\Pi}) = e^{i\frac{\sqrt{2}}{f}\mathbf{\Pi}\cdot T^{\mathbf{7}}} = \begin{bmatrix} \mathbb{I}_7 - \frac{\mathbf{\Pi}\mathbf{\Pi}^t}{\mathbf{\Pi}^t\cdot\mathbf{\Pi}}\left(1 - \cos\left(\frac{\sqrt{\mathbf{\Pi}^t\cdot\mathbf{\Pi}}}{f}\right)\right) & \frac{\mathbf{\Pi}}{\sqrt{\mathbf{\Pi}^t\cdot\mathbf{\Pi}}}\sin\left(\frac{\sqrt{\mathbf{\Pi}^t\cdot\mathbf{\Pi}}}{f}\right) \\ -\frac{\mathbf{\Pi}}{\sqrt{\mathbf{\Pi}^t\cdot\mathbf{\Pi}}}\sin\left(\frac{\sqrt{\mathbf{\Pi}^t\cdot\mathbf{\Pi}}}{f}\right) & \cos\left(\frac{\sqrt{\mathbf{\Pi}^t\cdot\mathbf{\Pi}}}{f}\right) \end{bmatrix}. \tag{A5}$$

The latter transforms nonlinearly under the action of an $SO(8)$ group element g, according to the standard relation:

$$\Sigma(\mathbf{\Pi}) \to g\cdot\Sigma(\mathbf{\Pi})\cdot h^{\dagger}(\mathbf{\Pi}, g), \tag{A6}$$

where $h(\mathbf{\Pi}, g) \in SO(7)$ depends on g and $\mathbf{\Pi}(x)$. We identify the Higgs boson with the NGB along the generator $T^{\mathbf{7}}_4$; in the unitary gauge, all the remaining NGBs are nonpropagating fields and the $\mathbf{\Pi}$ vector becomes

$$\mathbf{\Pi}|_{\text{unitary gauge}} = (0,\ldots,\pi_4 = \langle h\rangle + h(x),\ldots,0), \tag{A7}$$

where $\xi = \sin^2(\langle h\rangle/f) = v^2/f^2$. In this case the Σ matrix simplifies to:

$$\Sigma(\mathbf{\Pi})|_{\text{unitary gauge}} = e^{i\frac{\sqrt{2}}{f}\pi_4 T^{\mathbf{7}}_4} = \begin{bmatrix} \mathbb{I}_3 & 0 & 0 & 0 \\ 0 & \cos\frac{\pi_4}{f} & 0 & \sin\frac{\pi_4}{f} \\ 0 & 0 & \mathbb{I}_3 & 0 \\ 0 & -\sin\frac{\pi_4}{f} & 0 & \cos\frac{\pi_4}{f} \end{bmatrix}. \tag{A8}$$

Given the above symmetry breaking pattern, it is possible to define a LR parity,

$$P_{LR} = \text{diag}(-1,-1,-1,+1,-1,-1,-1,+1), \tag{A9}$$

which exchanges $SU(2)_L$ with $SU(2)_R$ inside $SO(4)$ and $\widetilde{SU}(2)_L$ with $\widetilde{SU}(2)_R$ inside $\widetilde{SO}(4)$. The corresponding action on the fields is such that π_4 is even, while all the other NGBs are odd. As already noticed in Sec. V C, P_{LR} is an element of both $SO(8)$ and $SO(7)$, which means that it is an exact symmetry of the strong dynamics and acts linearly on the physical spectrum of fields.

The CCWZ variables d_μ and E_μ are defined as usual through the Maurer-Cartan form,

$$\Sigma^{\dagger}(\mathbf{\Pi})D_\mu\Sigma(\mathbf{\Pi}) \equiv i d^i_\mu(\mathbf{\Pi})T^{\mathbf{7}}_i + iE^a_\mu(\mathbf{\Pi})T^{\mathbf{21}}_a, \tag{A10}$$

as the components along the broken and unbroken generators of $SO(8)$ respectively. The derivative D_μ is covariant with respect to the external SM and twin gauge fields:

$$D_\mu = \partial_\mu - iA^A_\mu T^A, \quad \text{with}$$
$$A^A_\mu T^A = g_2 W^{\alpha}_\mu (T_{\mathbf{L}})^{\alpha} + g_1 B_\mu (T_{\mathbf{R}})^3 + \tilde{g}_2 \tilde{W}^{\alpha}_\mu (\tilde{T}_{\mathbf{L}})^{\alpha}. \tag{A11}$$

Under the action of a global element $g \in SO(8)$, d_μ and E_μ transform with the rules of a local $SO(7)$ transformation:

$$d_\mu \equiv d^i_\mu T^{\mathbf{7}}_i \to h(\mathbf{\Pi}, g) d_\mu h^{\dagger}(\mathbf{\Pi}, g),$$
$$E_\mu \equiv E^a_\mu T^{\mathbf{21}}_a \to h(\mathbf{\Pi}, g)(E_\mu - i\partial_\mu)h^{\dagger}(\mathbf{\Pi}, g). \tag{A12}$$

It is straightforward to derive the explicit expressions of d_μ and E_μ from the Maurer-Cartan relation in Eq. (A10). They are however lengthy and not very illuminating, so we do not report them here. We can easily obtain the mass spectrum of the gauge sector of our theory from the NGB kinetic term;

in the unitary gauge and after rotating to the mass eigenstate basis, we find:

$$\mathcal{L}_{\rm mass} = \frac{f^2}{4}(d^i_\mu)^2 \supset \frac{g_2^2}{4} f^2 \xi W^+_\mu W^{\mu -} + \frac{(g_1^2+g_2^2)}{8} f^2 \xi Z^\mu Z_\mu + \frac{\tilde{g}_2^2}{8} f^2 (1-\xi) \sum_{i=1}^{3} (\tilde{W}^i_\mu)^2. \tag{A13}$$

APPENDIX B: MASS MATRICES AND SPECTRUM

In this Appendix, we briefly discuss the mass matrices of the different charged sectors in the composite TH model and the related particle spectrum. We refer to Ref. [13] for the expressions of the $\Psi_{\mathbf{7}}$ and $\tilde{\Psi}_{\mathbf{7}}$ multiplets in terms of their component heavy fermions.

We start by considering the fields that do not have the right quantum numbers to mix with the elementary SM and twin quarks and whose mass is therefore independent of the mixing parameters $y_{L,R}$ and $\tilde{y}_{L,R}$. These are the composite fermions $X_{5/3}$, $\tilde{D}_1$ and $\tilde{D}_{-1}$, with charges $5/3$, 1 and -1 respectively; their mass is exactly given by the Lagrangian parameters M_Ψ (for the first one), and $\tilde{M}_\Psi$ (for the last two).

The remaining sectors have charge $-1/3$, 0, and $2/3$ and because of the elementary/composite mixing the associated mass matrices are in general nondiagonal and must be diagonalized by a proper field rotation. The simplest case is the $(-1/3)$-charged sector, containing the bottom quark and the heavy B field; the mass matrix in the $\{b, B\}$ basis is

$$M_{-1/3} = \begin{pmatrix} 0 & f y_L \\ 0 & -M_\Psi \end{pmatrix}. \tag{B1}$$

After rotation, we find a massless bottom quark (it has no mass since we are not including the b_R in the model), and a massive B particle with $m_B^2 = M_\Psi^2 + y_L^2 f^2$.

As regards the sector of charge $2/3$, it contains seven different particles: the top quark, the toplike heavy states T and $X_{2/3}$ and four composite fermions that do not participate in the SM weak interactions, $S^1_{2/3}, \cdots S^4_{2/3}$. In the $\{t, T, X_{2/3}, S^1_{2/3}, \ldots, S^4_{2/3}\}$ basis, the mass matrix is given by:

$$M_{2/3} = \begin{pmatrix} 0 & \frac{1}{2} f y_L (\sqrt{1-\xi}+1) & -\frac{1}{2} f y_L (\sqrt{1-\xi}-1) & 0 & -\frac{f y_L \sqrt{\xi}}{\sqrt{2}} \\ 0 & -M_\Psi & 0 & 0 & 0 \\ 0 & 0 & -M_\Psi & 0 & 0 \\ 0 & 0 & 0 & -M_\Psi \times \mathbb{I}_3 & 0 \\ f y_R & 0 & 0 & 0 & -M_S \end{pmatrix}. \tag{B2}$$

The states $S^1_{2/3}, S^2_{2/3}, S^3_{2/3}$ completely decouple from the elementary sector and do not mix with the top quark. Their mass is therefore exactly given by the Lagrangian parameter M_Ψ. The remaining 4×4 matrix is in general too complicated to be analytically diagonalized, but one can easily find the spectrum in perturbation theory by expanding $M_{2/3}$ for $\xi \ll 1$, which is in general a phenomenologically viable limit. The leading order expression for the masses is then:

$$\begin{aligned} m_t^2 &\simeq \frac{f^4}{2} \frac{y_L^2 y_R^2}{M_S^2 + y_R^2 f^2} \xi + O(\xi^2), \\ m^2_{X_{2/3}} &= M_\Psi^2, \\ m_T^2 &\simeq M_\Psi^2 + y_L^2 f^2 \left(1 - \frac{\xi}{2}\right) + O(\xi^2), \\ m^2_{S^4_{2/3}} &\simeq M_S^2 + y_R^2 f^2 + \frac{y_L^2 f^2 M_S^2}{2(M_S^2 + y_R^2 f^2)} \xi + O(\xi^2). \end{aligned} \tag{B3}$$

The $X_{2/3}$ fermion can be also decoupled and its mass is exactly equal to M_Ψ. On the contrary, the other three particles mix with each other and their mass gets corrected after EWSB (as expected, the top mass is generated for nonzero values of ξ).

Finally, we analyze the neutral sector of our model. It comprises eight fields, the twin top and bottom quarks, and six of the composite fermions contained in the $\tilde{\Psi}_{\mathbf{7}}$ multiplet. Working in the field basis $\{\tilde{t}, \tilde{b}, \tilde{D}^1_0, \tilde{D}^2_0, \tilde{U}^1_0, \ldots, \tilde{U}^4_0\}$, the mass matrix reads:

$$M_0 = \begin{pmatrix} 0 & 0 & -\frac{1}{2}f\sqrt{\xi}\tilde{y}_L & \frac{1}{2}f\sqrt{\xi}\tilde{y}_L & 0 & 0 & -\frac{if\tilde{y}_L}{\sqrt{2}} & -\frac{f\sqrt{1-\xi}\tilde{y}_L}{\sqrt{2}} \\ 0 & 0 & 0 & 0 & -\frac{if\tilde{y}_L}{\sqrt{2}} & \frac{f\tilde{y}_L}{\sqrt{2}} & 0 & 0 \\ 0 & 0 & -\tilde{M}_\Psi & 0 & 0 & 0 & 0 & 0 \\ 0 & 0 & 0 & -\tilde{M}_\Psi & 0 & 0 & 0 & 0 \\ 0 & 0 & 0 & 0 & -\tilde{M}_\Psi & 0 & 0 & 0 \\ 0 & 0 & 0 & 0 & 0 & -\tilde{M}_\Psi & 0 & 0 \\ 0 & 0 & 0 & 0 & 0 & 0 & -\tilde{M}_\Psi & 0 \\ f\tilde{y}_R & 0 & 0 & 0 & 0 & 0 & 0 & -\tilde{M}_S \end{pmatrix}. \tag{B4}$$

After diagonalization, we find one massless eigenvalue corresponding to the twin bottom quark (it does not acquire mass since we are not introducing the $\tilde{b}_R$ field). Four of the neutral heavy fermions completely decouple and acquire the following masses

$$m_{\tilde{U}_0^1} = m_{\tilde{U}_0^3} = m_{\tilde{D}_0^2} = \tilde{M}_\Psi, \quad m^2_{\tilde{U}_0^2} = \tilde{M}_\Psi^2 + \tilde{y}_L^2 f^2. \tag{B5}$$

The elementary/composite mixing induces instead corrections to the masses of the remaining neutral particles; at leading order in ξ we find:

$$\begin{aligned} m_t^2 &\simeq \frac{f^4}{2}\frac{\tilde{y}_L^2\tilde{y}_R^2}{\tilde{M}_S^2 + \tilde{y}_R^2 f^2}(1-\xi) + O(\xi^2), \\ m^2_{\tilde{D}_0^1} &\simeq \tilde{M}_\Psi{}^2 + \frac{1}{2}\tilde{y}_L{}^2 f^2(1+\xi) + O(\xi^2), \\ m^2_{\tilde{U}_0^4} &\simeq \tilde{M}_S{}^2 + \tilde{y}_R^2 f^2 + \frac{\tilde{y}_L^2 f^2 \tilde{M}_S^2}{2(\tilde{M}_S^2 + \tilde{y}_R^2 f^2)}(1-\xi) + O(\xi^2). \end{aligned} \tag{B6}$$

We conclude by noticing that the masses of the particles in different charged sectors are not unrelated to each other, but must be connected according to the action of the twin symmetry. In particular, it is obvious that the two singlets $S^4_{2/3}$ and $\tilde{U}_0^4$ form an exact twin pair, as it is the case for each SM quark and the corresponding twin partner. The remaining pairs can be easily found from the spectrum and correspond to the implementation of the twin symmetry in the composite sector as defined in [13].

APPENDIX C: RG IMPROVEMENT OF THE HIGGS EFFECTIVE POTENTIAL

In this Appendix we describe the computation of the Higgs effective potential and its RG improvement. First of all, the UV threshold correction can be computed with a standard Coleman-Weinberg (CW) procedure, from which we can easily derive the function F_1 of Eq. (4.2). We find:

$$\begin{aligned} F_1 = -\frac{1}{4}\Bigg[1 &+ \frac{M_S^4}{(M_S^2 + f^2 y_R^2)^2} - \frac{M_S^2 + M_\Psi^2 - f^2 y_R^2}{M_S^2 - M_\Psi^2 + f^2 y_R^2}\log\frac{m_*^2}{M_\Psi^2} \\ &+ \frac{M_S^2(M_S^2(M_\Psi^2 + f^2 y_R^2) + 2f^2 y_R^2 M_\Psi^2 + M_S^4)}{(M_S^2 + f^2 y_R^2)^2(M_S^2 - M_\Psi^2 + f^2 y_R^2)}\log\frac{m_*^2}{M_S^2 + f^2 y_R^2}\Bigg]. \end{aligned} \tag{C1}$$

The IR contribution to the Higgs mass can be organized using a joint expansion in ξ and $(\alpha_i \log)$, where $\alpha_i = g_i^2/(4\pi)$ for couplings g_i. Schematically:

$$\begin{aligned} \delta m_h^2|_{\rm IR} = m_t^2 \frac{\alpha_t}{4\pi} t \Bigg[a_1 &+ b_1\xi + b_2\frac{\alpha_t}{4\pi}t + b_3\frac{\alpha_S}{4\pi}t + c_1\xi^2 + c_2\xi\frac{\alpha_S}{4\pi}t + c_3\frac{\alpha_S^2}{16\pi^2}t^2 \\ &+ c_4\xi\frac{\alpha_t}{4\pi}t + c_5\frac{\alpha_t^2}{16\pi^2}t^2 + c_6\frac{\alpha_t}{4\pi}\frac{\alpha_S}{4\pi}t^2\Bigg] - a_2 m_W^2\frac{\alpha_{\rm EW}}{4\pi}t + \text{twin}, \end{aligned} \tag{C2}$$

where $t = \log m_*^2/m_t^2$ and all the couplings are evaluated at the scale m_*. Here a_i, b_i, c_i are the $O(1)$ coefficients of the LO, NLO, and NNLO terms respectively. The twin contribution is obtained by substituting all α_i, a_i, b_i, c_i with the corresponding tilded quantities and t with $\tilde{t} = \log m_*^2/m_{\tilde{t}}^2$. The calculation of the LO and NLO terms is straightforward and all these contributions are included in our calculation. The NNLO terms indicated in blue are also simple to evaluate, and are included in our final result, indicated as NNLO*. The calculation of the remaining NNLO terms is more complicated, since it involves the running of several higher dimensional operators involving both the SM and twin fields. An attempt to compute the full potential at NNLO has been presented in Ref. [46]. However, while that result includes the contribution of the SM Goldstone bosons, additional contributions induced by the twin Goldstones, which are expected to arise at NNLO, are not included. Since the full calculation at NNLO is beyond the scope of this paper, we limit ourselves to only include the colored contributions in Eq. (C2). Comparing with Ref. [46] suggests that our NNLO* result gives an overestimate of the IR Higgs mass; that this is the case at large m_* is also evident from Fig. 1. For this reason we consider the NNLO* curve only as an indication of the importance of the NNLO correction, and use as final input for our numerical analysis the average of the LO and NLO results as described in Sec. IV.

We present now a procedure for computing the aforementioned contributions to the Higgs mass based on the approach of Ref. [46]. The RG improvement of the Higgs effective potential can be obtained by solving the one-loop β-function of the vacuum energy in the background of the Higgs field. The fermion contribution to the vacuum energy is given by

$$\frac{dV_f(h_c,t)^{\rm impr}}{dt} = \frac{N_c}{16\pi^2}[M_t(h_c,t)^4 + M_{\tilde{t}}(h_c,t)^4], \quad \text{(C3)}$$

whereas the leading gauge contribution is given by

$$V_g(h_c,t) = \frac{3}{16\pi^2}[2M_W(h_c)^2 + M_Z(h_c)^2 + 3M_{\tilde{W}}(h_c)^2]t. \quad \text{(C4)}$$

In order to compute the improved potential to NNLO* accuracy, we must input the gauge boson masses at tree-level and the renormalized top and twin top masses with leading-log accuracy in the corresponding Yukawa couplings and with next-to-leading-log accuracy in the strong gauge couplings. After solving Eq. (C3) for the effective potential, one must properly account for the Higgs wave function renormalization before expanding around the minimum of the potential in order to compute the physical Higgs mass. We fill in the salient details below.

On integrating out the heavy degrees of freedom, the composite twin Higgs model at the scale m_* can be represented by an effective Lagrangian that is invariant under a global $SU(3)_c \times SU(2)_L \times U(1)_Y$ symmetry, identified with the gauge group of the SM, as well as an additional $\widetilde{SU(3)}_c \times \widetilde{SU(2)}_{L+R}$. $\widetilde{SU(3)}_c$ is the gauged twin color and $\widetilde{SU(2)}_{L+R}$ is a global twin custodial group, broken only by fermion interactions, under which the twin gauge bosons ($\tilde{W}$) and Goldstone bosons (GBs) transform as triplets. We work in the gaugeless limit $g = g' = \tilde{g} = 0$, since we are only interesting in capturing the leading contributions to the Higgs potential that parametrically depend on y_t, $\tilde{y}_t$, g_S, and $\tilde{g}_S$.

The relevant light degrees of freedom are the SM fermion doublet, Q_L, and singlet, t_R, and their twin counterparts $\tilde{t}_L$ and $\tilde{t}_R$, the gluons and their twins; the Higgs doublet (including the massless GBs) and the twin GBs. For economy of notation we define a twin Higgs doublet in analogy with the SM one,

$$\tilde{H} = \frac{1}{\sqrt{2}}\begin{pmatrix} \sqrt{2}\tilde{\pi}^+ \\ \tilde{h} + i\tilde{\pi}^0 \end{pmatrix}, \quad \text{with} \quad \tilde{h} = f\sqrt{1 - \frac{2H^\dagger H + \tilde{\pi}^2}{f^2}}, \quad \text{(C5)}$$

making explicit the dependence on the twin Higgs which is integrated out at tree-level, thus realizing the $SO(8)$ symmetry nonlinearly.

Since the background field calculation at leading-log order requires corrections to the fermion masses and Higgs wave function at only one loop, we can neglect in the effective Lagrangian at the scale m_*, any operator that has vanishing coefficients at tree level. We also omit all operators that cannot be predicted solely in terms of the low-energy parameters of the theory (y_t and $\tilde{y}_t$) and f, including products of Higgs and fermion currents that arise from integrating out composite fermions.[17] We make the following field redefinition:

$$f\frac{\sin(\frac{|\Pi|}{f})}{|\Pi|}\Pi^i \to \Pi^i, \quad \text{for } |\Pi| = \sqrt{2H^\dagger H + \tilde{\pi}^2} \quad \text{(C6)}$$

which allows the effective Lagrangian, containing a pure scalar sector $\mathcal{L}_S$ and a fermionic sector $\mathcal{L}_F$, to be expressed in an especially compact form. The relevant operators in each sector are given below:

$$\mathcal{L}_S = D_\mu H^\dagger D^\mu H + \frac{1}{2}\partial_\mu\tilde{\pi}\partial^\mu\tilde{\pi} + \frac{c_H\mathcal{O}_H + c_{H\tilde{\pi}}\mathcal{O}_{H\tilde{\pi}} + c_{\tilde{\pi}}\mathcal{O}_{\tilde{\pi}}}{2f^2} + 2d_H\frac{H^\dagger H}{f^2}\mathcal{O}_H, \quad \text{(C7)}$$

[17] In any case, these do not contribute to the effective potential at this order.

and

$$\begin{aligned}\mathcal{L}_F = {} & i\bar{b}_L\not{\partial} b_L + i\bar{b}_R\not{\partial} b_R + i\bar{t}_L\not{\partial} t_L + i\bar{t}_R\not{\partial} t_R \\ & - y_t[\bar{Q}_L H^c t_R + \text{H.c.}] \\ & + i\bar{\tilde{b}}_L\not{\partial}\tilde{b}_L + i\bar{\tilde{b}}_R\not{\partial}\tilde{b}_R + i\bar{\tilde{t}}_L\not{\partial}\tilde{t}_L + i\bar{\tilde{t}}_R\not{\partial}\tilde{t}_R \\ & - \tilde{y}_t[\bar{\tilde{Q}}_L\tilde{H}^c\tilde{t}_R + \text{H.c.}].\end{aligned} \tag{C8}$$

where

$$\begin{aligned}\mathcal{O}_H &= \partial_\mu(H^\dagger H)\partial^\mu(H^\dagger H), \\ \mathcal{O}_{\tilde{\pi}} &= \partial_\mu\tilde{\pi}^2\partial^\mu\tilde{\pi}^2, \\ \mathcal{O}_{H\tilde{\pi}} &= \partial_\mu(H^\dagger H)\partial^\mu\tilde{\pi}^2.\end{aligned} \tag{C9}$$

We have defined a twin fermion doublet $\tilde{Q}_L = (\tilde{t}_L, \tilde{b}_L)^T$, transforming under the twin-sector symmetries, and the Yukawa couplings are defined at tree-level as

$$y_t(m_*) = \frac{y_L y_R f}{\sqrt{M_S^2 + y_R^2 f^2}} \quad \text{and} \quad \tilde{y}_t(m_*) = \frac{y_{\tilde{L}} y_{\tilde{R}} f}{\sqrt{\tilde{M}_S^2 + y_{\tilde{R}}^2 f^2}}. \tag{C10}$$

The Wilson coefficients at the scale m_* have the boundary values:

$$c_H(m_*) = c_{H\tilde{\pi}}(m_*) = c_{\tilde{\pi}}(m_*) = d_H(m_*) = 1, \tag{C11}$$

while the Z_2 symmetry enforces

$$y_t(m_*) = \tilde{y}_t(m_*) \quad \text{and} \quad \alpha_s(m_*) = \widetilde{\alpha}_s(m_*) \tag{C12}$$

We now expand the effective Lagrangian in the background of the Higgs field $h = h_c + \hat{h}$ to obtain:

$$\begin{aligned}\mathcal{L}_S = {} & Z_\pi(h_c)\left(\frac{1}{2}\partial_\mu\pi^0\partial^\mu\pi^0 + \partial_\mu\pi^+\partial^\mu\pi^-\right) \\ & + \frac{1}{2}Z_{\hat{h}}(h_c)\partial_\mu\hat{h}\partial^\mu\hat{h} + \frac{1}{2}Z_{\tilde{\pi}}(h_c)\partial_\mu\tilde{\pi}\partial^\mu\tilde{\pi},\end{aligned} \tag{C13}$$

where we defined

$$\begin{aligned}&Z_\pi(h_c) = 1, \qquad Z_{\hat{h}}(h_c) = 1 + c_H\frac{h_c^2}{f^2} + d_H\frac{h_c^4}{f^4}, \\ &Z_{\tilde{\pi}}(h_c) = 1,\end{aligned} \tag{C14}$$

and

$$\begin{aligned}\mathcal{L}_F = {} & \sum_\psi iZ_\psi(h_c)\bar{\psi}\not{\partial}\psi - m_t(h_c)\bar{t}t - m_b(h_c)\bar{b}b - m_{\tilde{t}}(h_c)\bar{\tilde{t}}\tilde{t} - m_{\tilde{b}}(h_c)\bar{\tilde{b}}\tilde{b} \\ & - \frac{y_t(h_c)}{\sqrt{2}}\hat{h}\,\bar{t}\,t - \frac{iy_t(h_c)}{\sqrt{2}}\pi^0\bar{t}\gamma^5 t - \frac{iy_t(h_c)}{2}\pi^-\bar{b}(1+\gamma^5)t + \frac{iy_t(h_c)}{2}\pi^+\bar{t}(1-\gamma^5)b \\ & + \frac{\tilde{y}_t(h_c)}{\sqrt{2}}\hat{h}\,\bar{\tilde{t}}\,\tilde{t} - \frac{iy_{\tilde{\pi}\tilde{t}\tilde{t}}(h_c)}{\sqrt{2}}\tilde{\pi}^0\bar{\tilde{t}}\gamma^5\tilde{t} - \frac{iy_{\tilde{\pi}\tilde{t}\tilde{b}}(h_c)}{2}\tilde{\pi}^-\bar{\tilde{b}}(1+\gamma^5)\tilde{t} + \frac{iy_{\tilde{\pi}\tilde{t}\tilde{b}}(h_c)}{2}\tilde{\pi}^+\bar{\tilde{t}}(1-\gamma^5)\tilde{b}.\end{aligned} \tag{C15}$$

Here ψ runs over all the Weyl fermions $\{t_L, t_R, b_L, b_R, \tilde{t}_L, \tilde{t}_R, \tilde{b}_L, \tilde{b}_R\}$ and we defined

$$\begin{aligned}&Z_\psi(h_c) = 1, \qquad y_t(h_c) = y_t, \qquad m_t(h_c) = \frac{y_t h_c}{\sqrt{2}}, \qquad m_b(h_c) = 0, \\ &y_{\tilde{\pi}\tilde{t}\tilde{b}}(h_c) = \tilde{y}_t, \qquad \tilde{y}_t(h_c) = \frac{\tilde{y}_t h_c}{f}\frac{1}{\sqrt{1-\frac{h_c^2}{f^2}}}, \qquad m_{\tilde{t}}(h_c) = \frac{\tilde{y}_t f}{\sqrt{2}}\sqrt{1-\frac{h_c^2}{f^2}} \qquad m_{\tilde{b}}(h_c) = 0.\end{aligned} \tag{C16}$$

We can now compute the running masses of the top and twin top in the background:

$$M_t(h_c, t) \approx m_t(h_c)\left[1 + \left(\frac{g_S^2}{4\pi^2} - \frac{3y_t(h_c)^2}{4(4\pi)^2 Z_{\hat{h}}(h_c)}\right)t + \frac{22g_S^4}{(4\pi)^4}t^2\right], \tag{C17a}$$

$$M_{\tilde{t}}(h_c, t) \approx m_{\tilde{t}}(h_c)\left[1 + \left(\frac{\tilde{g}_S^2}{4\pi^2} - \frac{3\tilde{y}_t(h_c)^2}{4(4\pi)^2 Z_{\hat{h}}(h_c)}\right)t + \frac{22\tilde{g}_S^4}{(4\pi)^4}t^2\right], \tag{C17b}$$

with $t = \log(m_*^2/\mu^2)$. The values of the parameters in the Higgs background are simply read off from the effective Lagrangian at the scale m_*. Notice that in the background, only y_t and $\tilde{y}_t$ are scale-dependent, while h_c is "frozen"; hence the running of the quark mass is identical to that of the corresponding Yukawa coupling.

We can now substitute Eqs. (C17) into the RG equation (C3), integrate the result and expand at the required order in h_c/f to get

$$V_f(h_c,t)^{\rm impr} = \frac{N_c}{64\pi^2}\left\{\left[y_t^4 h_c^4 + \tilde{y}_t^4 f^4\left(1-\frac{h_c^2}{f^2}\right)^2\right]t + \frac{y_t^4 h_c^4}{2}\left(\frac{g_S^2}{\pi^2}-\frac{3y_t^2}{(4\pi)^2}\right)t^2 + \frac{23}{96\pi^4}\left[g_S^4 y_t^4 h_c^4 + \tilde{g}_S^4\tilde{y}_t^4 f^4\left(1-\frac{h_c^2}{f^2}\right)^2\right]t^3 + \frac{\tilde{y}_t^4 f^4}{32\pi^2}\left(1-\frac{h_c^2}{f^2}\right)^2\left[16\tilde{g}_S^2 - 3\tilde{y}_t^2\frac{h_c^2}{f^2}\left(1-(1+c_H)\frac{h_c^2}{f^2}\right)\right]t^2\right\}. \tag{C18}$$

This is the improved effective potential written in terms of parameters computed at the scale m_*. We can now treat h_c as a quantum field, fluctuating around its minimum $h_c = h + \langle h\rangle$. We then have to take into account that the potential (C18) has been computed in a noncanonical basis for h_c, where its kinetic term coefficient, including only the leading logarithmic running, is

$$Z_{h_c}(t) = 1 + \frac{3y_t^2}{(4\pi)^2}t. \tag{C19}$$

Notice that only the top contributes to the one-loop running of the h_c wave function, since the twin top only couples quadratically to h_c, giving rise to a one-loop contribution that is not logarithmically divergent. After normalizing h_c using Eq. (C19), including a Z_2 breaking mass term necessary to achieve a viable minimum and minimizing the potential, h_c acquires a vacuum expectation value $h_c = h + \langle h\rangle$. This makes the wave function of h (the Higgs field in the minimum) noncanonical again, due to the presence of c_H:

$$Z_h(\langle h\rangle) = 1 + c_H\frac{\langle h\rangle^2}{f^2}. \tag{C20}$$

After normalizing h taking into account also this last effect, and including the LO gauge contribution, the desired contribution to the Higgs mass reads:

$$\delta m_h^2|_{\rm IR} = \frac{3v^2}{8\pi^2}\left\{(y_t^4 t + y_{\tilde{t}}^4\tilde{t})(1 - c_H\xi + (c_H^2 - d_H)\xi^2) - \frac{1}{16}[(3g_2^4 + 2g_1^2 g_2^2 + g_1^4)t + 3\tilde{g}_2^4\tilde{t}] + \frac{1}{32\pi^2}(16y_t^4 g_S^2 t^2 + 16y_{\tilde{t}}^4\tilde{g}_S^2\tilde{t}^2)(1 - c_H\xi) + \frac{1}{32\pi^2}(-15y_t^6 t^2 - 12y_t^2\tilde{y}_t^4\tilde{t}^2 + 3y_{\tilde{t}}^6\tilde{t}^2(1+c_H)) + \frac{23}{96\pi^4}(y_t^4 g_S^4 t^3 + y_{\tilde{t}}^4\tilde{g}_S^4\tilde{t}^3)\right\}, \tag{C21}$$

where we have highlighted the various contributions present in Eq. (C2) with the corresponding colors and set $t = \log m_*^2/m_t^2$, $\tilde{t} = \log m_*^2/m_{\tilde{t}}^2$. The Higgs vev has been defined by fixing the W mass according to

$$m_W^2 = \frac{g^2\langle h\rangle^2}{4}, \qquad \Rightarrow \langle h\rangle^2 = v^2 = \frac{1}{\sqrt{2}G_F} = 246\ \text{GeV}. \tag{C22}$$

A numerical determination of the IR contribution $\delta m_h^2|_{\rm IR}$ can be obtained by making use of the experimental value of the top quark mass to fix $y_t(m_*)$ and $\tilde{y}_t(m_*)$. In fact, the 1-loop RG equation for y_t is decoupled from the twin sector at the order we are interested in and can be easily solved. Including only the orders required to match our calculation of the Higgs mass squared in Eq. (C21) we get:

$$y_t(m_*) = y_{\tilde{t}}(m_*) = y_t(m_t)\left[1 - \left(\frac{g_S(m_t)^2}{4\pi^2} - \frac{9y_t(m_t)^2}{64\pi^2}\right)\log\frac{m_*^2}{m_t^2} + \frac{22 g_S(m_t)^4}{(4\pi)^4}\log^2\frac{m_*^2}{m_t^2}\right],$$
$$g_S(m_*) = \tilde{g}_S(m_*) = g_S(m_t)\left[1 - \frac{7g_S(m_t)^2}{32\pi^2}\log\frac{m_*^2}{m_t^2}\right], \tag{C23}$$

which fixes $y_t(m_*)$ in terms of $y_t(m_t)$. As an input to our numerical analysis we use the PDG combination for the top quark pole mass $m_t = 173.21 \pm 0.51 \pm 0.71$ GeV [57]. This is converted into the top Yukawa coupling in the $\overline{\rm MS}$ scheme $y_t^{\overline{\rm MS}}(m_t) = 0.936 \pm 0.005$ by making use of Eq. (62) of Ref. [65]. We then use $y_t(m_t) = y_t^{\overline{\rm MS}}(m_t)$. For the strong interaction, we run the parameter measured at the scale of the Z boson mass, $g_S(m_Z) \sim 1.22$, to the scale m_t to obtain $g_S(m_t)$.

APPENDIX D: OPERATOR ANALYSIS OF THE HEAVY-VECTOR CONTRIBUTION TO δg_{Lb}

In this Appendix we discuss the UV threshold contribution to δg_{Lb} generated by the tree-level exchange of the composite vectors ρ [adjoint of $SO(7)$] and ρ^X [singlet of $SO(7)$] at zero transferred momentum. This effect arises at leading order from diagrams with a loop of heavy fermions, as in Fig. 5. Our simple effective operator analysis will show that the contribution of the ρ identically vanishes, in agreement with the explicit calculation in the simplified model.

An adjoint of $SO(7)$ decomposes under the custodial $SU(2)_L \times SU(2)_R$ as:

$$\mathbf{21} = (\mathbf{3},\mathbf{1}) + (\mathbf{1},\mathbf{3}) + 3 \times (\mathbf{2},\mathbf{2}) + 3 \times (\mathbf{1},\mathbf{1}). \tag{D1}$$

The first two representations contain the vector resonances that are typically predicted by ordinary CH models, namely ρ_L and ρ_R. They mix at tree-level with the Z boson and in general contribute to δg_{Lb}. The remaining resonances do not have the right quantum numbers to both mix with the Z boson and couple to the left-handed bottom quark due to isospin conservation. As a result, only the components ρ_L and ρ_R inside the **21** can give a contribution to δg_{Lb} at the 1-loop level.

In order to analyze such effect, we make use of an operator approach. We classify the operators that can be generated at the scale m_* by integrating out the composite states, focusing on those which can modify the $Zb\bar{b}$ vertex at zero transferred momentum. In general, since an exact P_{LR} invariance implies vanishing correction to g_{Lb} at zero transferred momentum, any δg_{Lb} must be generated proportional to some spurionic coupling breaking this symmetry. In our model, the only coupling breaking P_{LR} in the fermion sector is y_L, and a nonvanishing δg_{Lb} arises at order y_L^4. The effective operators can be constructed using the CCWZ formalism in terms of the covariant spurion

$$\chi_L = \Sigma^\dagger \Delta^\dagger \Delta \Sigma, \tag{D2}$$

where Δ is defined in Eq. (3.11). By construction χ_L is a Hermitian complex matrix. Under the action of an element $g \in SO(8)$, it transforms as a $\mathbf{21}_a + \mathbf{27}_s + \mathbf{7} + \mathbf{1} + \mathbf{1}$ of $SO(7)$ (where the 7 is complex), and its formal transformation rule is

$$\chi_L \to h(\mathbf{\Pi}, g) \chi_L h^\dagger(\mathbf{\Pi}, g), \qquad h \in SO(7). \tag{D3}$$

As a second ingredient to build the effective operators, we uplift the elementary doublet q_L into a $\mathbf{7} + \mathbf{1}$ representation of $SO(7)$ by dressing it with NGBs:

$$Q_L = (\Sigma^\dagger \Delta^\dagger q_L). \tag{D4}$$

We will denote with $Q_L^{(7)}$ and $Q_L^{(1)}$ respectively the septuplet and singlet components of Q_L. Since $Q_L^{(1)}$ does not contain b_L (it depends only on t_L), only $Q_L^{(7)}$ is of interest for the present analysis. Under a $SO(8)$ transformation

$$Q_L^{(7)} \to h(\mathbf{\Pi}, g) Q_L^{(7)}. \tag{D5}$$

The effective operators contributing to δg_{Lb} can be thus constructed in terms of χ_L, d_μ, and $Q_L^{(7)}$. We find that the exchange of ρ_μ in the diagram of Fig. 5 can generate two independent operators,

$$\begin{aligned} O_{21} &= \bar{Q}_L^{(7)} \gamma^\mu T^a Q_L^{(7)} \mathrm{Tr}(d_\mu \chi_L T^a), \\ O'_{21} &= \bar{Q}_L^{(7)} \gamma^\mu T^a Q_L^{(7)} (d_\mu T^a \chi_L)_{88}, \end{aligned} \tag{D6}$$

where T^a is an $SO(8)$ generator in the adjoint of $SO(7)$; the exchange of ρ_μ^X gives rise to other two[18]:

$$O_1 = \bar{Q}_L^{(7)} \gamma^\mu Q_L^{(7)} \mathrm{Tr}(d_\mu \chi_L), \qquad O'_1 = \bar{Q}_L^{(7)} \gamma^\mu Q_L^{(7)} (d_\mu \chi_L)_{88}. \tag{D7}$$

Simple inspection reveals that only the septuplet component of χ_L contributes in the above equations. One can easily check that the operators of Eq. (D6) give a vanishing contribution to δg_{Lb}. In particular, the terms generated by the exchange of the (2,2) and (1,1) components of the ρ give (as expected) an identically vanishing contribution. Those arising from ρ_L and ρ_R [obtained by setting T^a in Eq. (D6) equal to respectively one of the (3,1) and (1,3) generators] give instead an equal and opposite correction to g_{Lb}. This is in agreement with the results of a direct calculation in the simplified model, from which one finds

[18] Additional structures constructed in terms of d_μ and χ_L can be rewritten in terms of those appearing in Eqs. (D6) and (D7), hence they do not generate new linearly independent operators. Notice that $\mathrm{Tr}(d_\mu \chi_L T^a) \propto f^{a\hat{a}\hat{b}} d_\mu^{\hat{a}} (\chi_L^{(7)})^{\hat{b}}$, $(d_\mu T^a \chi_L)_{88} \propto f^{a\hat{a}\hat{b}} d_\mu^{\hat{a}} (\chi_L^{(7)*})^{\hat{b}}$, $(d_\mu \chi_L)_{88} = -d_\mu^{\hat{a}} (\chi_L^{(7)})^{\hat{a}}$, $\mathrm{Tr}(d_\mu \chi_L) = -d_\mu^{\hat{a}} (\chi_L^{(7)})^{\hat{a}} + d_\mu^{\hat{a}} (\chi_L^{(7)*})^{\hat{a}}$, where $\chi_L^{(7)}$ denotes the component of χ_L transforming as a (complex) fundamental of $SO(7)$. A similar classification in the context of $SO(5)/SO(4)$ models in Ref. [29] found only one operator, corresponding to the linear combination $O'_1 - O_1$.

that the contributions from ρ_L and ρ_R cancel each other. Finally, a nonvanishing δg_{Lb} arises from the operators of Eq. (D7) generated by the exchange of ρ^X. Upon expanding in powers of the Higgs doublet, O_1 and O_1' both match the dimension-6 operator O_{Hq} of Eq. (5.11) and differ only by higher-order terms.

APPENDIX E: EXPLICIT FORMULAS FOR THE EWPO

In this Appendix we report the results of our calculation of the electroweak precision observables, in particular we collect here the explicit expression of the coefficients $a_{\rm UV}$, $a_{\rm IR}$ of Eq. (5.12) and $b_{\rm UV}$, $c_{\rm UV}$, $b_{\rm IR}$ of Eq. (5.17).

Let us start considering the $\hat{T}$ parameter. For convenience, we split the UV contribution into two parts, redefining $a_{\rm UV}$ as:

$$a_{\rm UV} = a_{\rm UV}^{\rm Fin} + a_{\rm UV}^{\rm Log} \log\left(\frac{M_\Psi^2}{M_S^2 + f^2 y_R^2}\right). \tag{E1}$$

The coefficients $a_{\rm UV}^{\rm Fin}$ and $a_{\rm UV}^{\rm Log}$ are obtained through a straightforward calculation, but their expressions are complicated functions of the Lagrangian parameters. We thus show them only in the limit $c_L = c_R \equiv c$ and $M_\Psi = M_S \equiv M$, for simplicity. For $a_{\rm IR}$ we give instead the complete expression. We find:

$$\begin{aligned}
a_{\rm UV}^{\rm Fin} &= \frac{1}{12}\left(-\frac{12M^4}{f^4 y_R^4} + \frac{6f^2M^2y_R^2}{(f^2y_R^2+M^2)^2} + \frac{9M^6}{(f^2y_R^2+M^2)^3} - 8\right) \\
&\quad + \frac{c(-5f^8y_R^8 - 2f^6M^2y_R^6 + 7f^4M^4y_R^4 + 12f^2M^6y_R^2 + 4M^8)}{\sqrt{2}f^4y_R^4(f^2y_R^2+M^2)^2} \\
&\quad + \frac{c^2(f^2y_R^2+2M^2)^2(3f^2y_R^2-5M^2)}{2f^4y_R^4(f^2y_R^2+M^2)}, \\
a_{\rm UV}^{\rm Log} &= \frac{f^6y_R^6 - f^4M^2y_R^4 - f^2M^4y_R^2 - 2M^6}{2f^6y_R^6} \\
&\quad + \frac{\sqrt{2}c(2f^6y_R^6 - 3f^4M^2y_R^4 + 3f^2M^4y_R^2 + 2M^6)}{f^6y_R^6} + \frac{c^2(f^2M^4y_R^2 - 10M^6)}{f^6y_R^6}, \\
a_{\rm IR} &= \frac{1}{2} + \frac{M_S^2M_\Psi^2}{2(M_S^2+f^2y_R^2)^2} + \sqrt{2}\frac{c_LM_SM_\Psi + 2c_Rf^2y_R^2}{M_S^2+f^2y_R^2}.
\end{aligned} \tag{E2}$$

The derivation of δg_{b_L} at 1-loop level is more involved and requires the computation of a series of diagrams. As explained in the text, we focus on those featuring a loop of fermions and NGBs (see Fig. 4), and that one with a loop of fermion and the tree-level exchange of a heavy vector (see Fig. 5). The coefficients $c_{\rm UV}$ is generated only by the latter diagram; we find:

$$c_{\rm UV} = \alpha_{7L}(\alpha_{1R}+\alpha_{7R})(1+\sqrt{2}c_R)\frac{g_{\rho^x}^2f^2}{M_{\rho^x}^2}\frac{M_\Psi^2}{2(M_\Psi^2+y_L^2f^2)}. \tag{E3}$$

We remind the reader that in our numerical analysis we use $M_{\rho^x}/(g_{\rho^x}f) = 1$, see footnote 5. We redefine the other two coefficients as

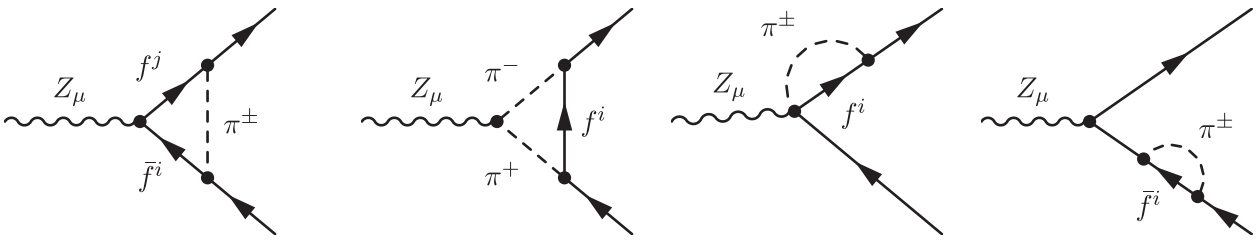

FIG. 4. Diagrams with a loop of fermions and NGBs contributing to the $Zb_L\bar{b}_L$ vertex. Here f^i indicates any fermion (both heavy and light) in our simplified model; $\pi^\pm$ are the charged NGBs.

$$b_{\rm IR} = \delta_{\rm IR} + \bar{\delta}_{\rm IR}$$
$$b_{\rm UV} = (\delta^{\rm Fin}_{\rm UV} + \bar{\delta}^{\rm Fin}_{\rm UV}) + (\delta^{\rm Log}_{\rm UV} + \bar{\delta}^{\rm Log}_{\rm UV}) \log\left(\frac{M_\Psi^2}{M_S^2 + f^2 y_R^2}\right), \tag{E4}$$

where $\delta_{\rm IR}$, $\delta^{\rm Fin}_{\rm UV}$, and $\delta^{\rm Log}_{\rm UV}$ are generated by the diagrams in Fig. 4 only, whereas $\bar{\delta}_{\rm IR}$, $\bar{\delta}^{\rm Fin}_{\rm UV}$, and $\bar{\delta}^{\rm Log}_{\rm UV}$ parametrize the correction due to the tree-level exchange of a heavy spin-1 singlet in Fig. 5. As before, we report the expression of the UV parameters in the limit $c_L = c_R \equiv c$, $M_\Psi = M_S \equiv M$, for simplicity; in the case of the coefficients with a bar, generated by the diagram of Fig. 5, we further set $\alpha_{7L} = \alpha_{1L}$ and $\alpha_{7R} = \alpha_{1R}$. We find:

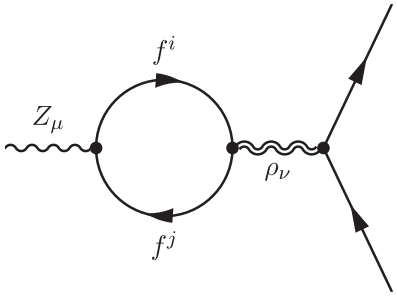

FIG. 5. The diagram contributing to $Zb_L\bar{b}_L$ with a loop of fermions and tree-level exchange of a heavy vector. Here f^i and f^j denote generic fermions in the theory, both heavy and light, whereas ρ_ν indicates the heavy vector.

$$\begin{aligned}
\delta^{\rm Fin}_{\rm UV} &= \frac{-2f^6y_R^6 - 4f^4M^2y_R^4 - 4f^2M^4y_R^2 + M^6}{12(f^2y_R^2 + M^2)^3} - \frac{c(f^6y_R^6 + 4f^4M^2y_R^4 - 2f^2M^4y_R^2 + M^6)}{6\sqrt{2}f^2y_R^2(f^2y_R^2 + M^2)^2} \\
&\quad + \frac{1}{6}c^2M^2\left(\frac{3}{f^2y_R^2 + M^2} - \frac{2}{f^2y_R^2}\right) - \frac{c^3M^2}{3\sqrt{2}f^2y_R^2}, \\
\delta^{\rm Log}_{\rm UV} &= \frac{1}{6} - \frac{M^2}{6f^2y_R^2} - \frac{c^3M^4}{3\sqrt{2}f^4y_R^4} - \frac{c^2M^4}{3f^4y_R^4} - \frac{c(-f^4y_R^4 + 2f^2M^2y_R^2 + M^4)}{6\sqrt{2}f^4y_R^4}, \\
\bar{\delta}^{\rm Fin}_{\rm UV} &= \frac{f^2M^2\alpha_{1L}g_{\rho^x}^2(f^4y_R^4(\alpha_{1L} + 2\alpha_{1R}) + f^2M^2y_R^2(3\alpha_{1L} + 8\alpha_{1R}) + 2M^4(\alpha_{1L} + \alpha_{1R}))}{4M_{\rho^x}^2(f^2y_L^2 + M^2)(f^2y_R^2 + M^2)^2} \\
&\quad + \frac{cf^2M^2\alpha_{1L}g_{\rho^x}^2(f^2y_R^2(2\alpha_{1L} + \alpha_{1R}) + 2M^2\alpha_{1L})}{\sqrt{2}M_{\rho^x}^2(f^2y_L^2 + M^2)(f^2y_R^2 + M^2)}, \\
\bar{\delta}^{\rm Log}_{\rm UV} &= \frac{cM^4\alpha_{1L}g_{\rho^x}^2(\alpha_{1L} - \alpha_{1R})}{\sqrt{2}y_R^2M_{\rho^x}^2(f^2y_L^2 + M^2)} + \frac{f^2M^2\alpha_{1L}\alpha_{1R}g_{\rho^x}^2}{2M_{\rho^x}^2(f^2y_L^2 + M^2)}.
\end{aligned} \tag{E5}$$

For the IR coefficients we give instead the full expressions. We find:

$$\begin{aligned}
\delta_{\rm IR} &= \frac{1}{6} + \frac{M_S^2M_\Psi^2}{6(M_S^2 + f^2y_R^2)^2} + \sqrt{2}\frac{c_LM_SM_\Psi}{3(M_S^2 + f^2y_R^2)} + \sqrt{2}\frac{c_Rf^2y_R^2}{12(M_S^2 + f^2y_R^2)}, \\
\bar{\delta}_{\rm IR} &= \alpha_{7L}\alpha_{1R}\frac{g_{\rho^x}^2}{M_{\rho^x}^2}\frac{f^4M_\Psi^2y_R^2}{2(f^2y_L^2 + M_\Psi^2)(f^2y_R^2 + M_S^2)}.
\end{aligned} \tag{E6}$$

Notice that the IR corrections $a_{\rm IR}$ and $b_{\rm IR}$ are related to each other and parametrize the running of the effective coefficients $\bar{c}_{Hq}$, $\bar{c}'_{Hq}$, and $\bar{c}_{Ht}$, as explained in the main text.

Finally, we report the contribution to $\hat{S}$ generated in our simplified model by loops of heavy fermions. We do not include this correction in our electroweak fit, because in the perturbative region of the parameter space it is subdominant with respect to the tree-level shift of Eq. (5.6). Rather, we use this computation as an additional way to estimate the perturbativity bound, as discussed in Sec. III B. Analogously to what we did for $\hat{T}$ and δg_{Lb}, we parametrize the fermionic contribution to $\hat{S}$ as:

$$\begin{aligned}
\Delta\hat{S}_\Psi &= \frac{g_2^2}{8\pi^2}\xi\left[(1 - c_L^2 - c_R^2)\log\frac{m_*^2}{M_\Psi^2} + (1 - \tilde{c}_L^2 - \tilde{c}_R^2)\log\frac{m_*^2}{\tilde{M}_\Psi^2}\right] \\
&\quad + \frac{g_2^2}{16\pi^2}\xi\left[s^{\rm Fin}_{\rm UV} + s^{\rm Log}_{\rm UV}\log\left(\frac{M_\Psi^2}{M_S^2 + f^2y_R^2}\right) + \tilde{s}^{\rm Fin}_{\rm UV} + \tilde{s}^{\rm Log}_{\rm UV}\log\left(\frac{\tilde{M}_\Psi^2}{\tilde{M}_S^2 + f^2\tilde{y}_R^2}\right)\right] \\
&\quad + \frac{g_2^2}{16\pi^2}\xi s_{\rm IR}\frac{y_L^2f^2}{M_\Psi^2}\log\frac{M_1^2}{m_t^2}.
\end{aligned} \tag{E7}$$

Terms in the first line are logarithmically sensitive to the UV cutoff, the second line contains the UV threshold corrections, while the IR running appears in the third line. The UV thresholds include a contribution from the twin composites $\tilde{\Psi}_7$ and $\tilde{\Psi}_1$, parametrized by $\tilde{s}_{\rm UV}^{\rm Fin}$ and $\tilde{s}_{\rm UV}^{\rm Log}$. At leading order in y_L, by virtue of the twin parity invariance of the strong sector, such a contribution can be obtained from that of Ψ_7 and Ψ_1 (i.e. from $s_{\rm UV}^{\rm Fin}$ and $s_{\rm UV}^{\rm Log}$) by simply interchanging the tilded quantities with the untilded ones. Higher orders in y_L break this symmetry and generate different corrections in the two sectors. We performed the computation of the UV coefficients for $y_L = 0$, whereas $s_{\rm IR}$ is derived up to order y_L^2. We find:

$$\begin{aligned}
s_{\rm UV}^{\rm Fin} &= \frac{1}{2} - \frac{6c_L c_R M_S M_\Psi (f^2 y_R^2 + M_S^2 + M_\Psi^2)}{(f^2 y_R^2 + M_S^2 - M_\Psi^2)^2} + \frac{(c_R^2 + c_L^2)}{6}\left(\frac{24 M_S^2 M_\Psi^2}{(f^2 y_R^2 + M_S^2 - M_\Psi^2)^2} - 7\right), \\
s_{\rm UV}^{\rm Log} &= -\frac{2(M_S^2 + f^2 y_R^2)}{(M_S^2 - M_\Psi^2 + f^2 y_R^2)^3}[6 c_L c_R M_S M_\Psi^3 + c_R^2 M_S^2 (f^2 y_R^2 + M_S^2 - 3M_\Psi^2) \\
&\quad + c_L^2 (f^2 y_R^2 + M_S^2)(f^2 y_R^2 + M_S^2 - 3M_\Psi^2)], \\
s_{\rm IR} &= \frac{M_S^2 M_\Psi^4 - f^2 y_L^2((f^2 y_R^2 + M_S^2)(M_S^2 - f^2 y_R^2) + M_S^2 M_\Psi^2) + M_\Psi^2 (f^2 y_R^2 + M_S^2)^2}{6 M_\Psi^2 (f^2 y_R^2 + M_S^2)^2} \\
&\quad - c_R \frac{2\sqrt{2} f^2 y_R^2 (M_\Psi^2 - f^2 y_L^2)}{3 M_\Psi^2 (f^2 y_R^2 + M_S^2)} - c_L \frac{\sqrt{2} M_S (M_\Psi^2 - f^2 y_L^2)}{3 M_\Psi (f^2 y_R^2 + M_S^2)}.
\end{aligned} \tag{E8}$$

APPENDIX F: THE EW FIT

For our analysis of the electroweak observables we make use of the fit to the parameters $\epsilon_{1,2,3,b}$ [66–68] performed in Ref. [69] (see also Ref. [26]). The central values there obtained for the shifts $\Delta\epsilon_i \equiv \epsilon_i - \epsilon_i^{\rm SM}$ and the corresponding correlation matrix are

$$\begin{aligned}
\Delta\epsilon_1 &= 0.0007 \pm 0.0010 \\
\Delta\epsilon_2 &= -0.0001 \pm 0.0009 \\
\Delta\epsilon_3 &= 0.0006 \pm 0.0009 \\
\Delta\epsilon_b &= 0.0003 \pm 0.0013
\end{aligned} \qquad \rho = \begin{pmatrix} 1 & 0.8 & 0.86 & -0.33 \\ 0.8 & 1 & 0.51 & -0.32 \\ 0.86 & 0.51 & 1 & -0.22 \\ -0.33 & -0.32 & -0.22 & 1 \end{pmatrix}. \tag{F1}$$

We can directly relate $\Delta\epsilon_1$ to $\Delta\hat{T}$ and $\Delta\epsilon_3$ to $\Delta\hat{S}$ by using the results of Refs. [45,47], and furthermore $\Delta\epsilon_b = -2\delta g_{b_L}$. We set $\Delta\epsilon_2 = 0$ in our study, since its effect is subdominant in our model as well as in CH models [47]. We thus make use of Eq. (F1) to perform a χ^2 test of the compatibility of our predictions with the experimental constraints. The χ^2 function is defined as usual:

$$\chi^2 = \sum_{ij} (\Delta\epsilon_i - \mu_i)(\sigma^2)_{ij}^{-1} (\Delta\epsilon_j - \mu_j), \qquad (\sigma)_{ij}^2 = \sigma_i \rho_{ij} \sigma_j, \tag{F2}$$

where μ_i and σ_i denote respectively the mean values and the standard deviations of Eq. (F1), while $\Delta\epsilon_i$ indicates the theoretical prediction for each EW observable computed in terms of the Lagrangian parameters. After deriving the χ^2, we perform a fit by scanning over the points in our parameter space keeping only those for which $\Delta\chi^2 \equiv \chi^2 - \chi^2_{\rm min} < 7.82$, the latter condition corresponding to the 95% confidence level with 3 degrees of freedom. Using this procedure, we convert the experimental constraints into bounds over the plane (M_Ψ, ξ).

APPENDIX G: ESTIMATES OF THE PERTURBATIVITY BOUND

This Appendix contains details on the derivation of the perturbative limits discussed in Sec. III B. As explained there, we consider the processes $\pi^a\pi^b \to \pi^c\pi^d$ and $\pi^a\pi^b \to \bar{\psi}^c\psi^d$, where $\psi = \{\Psi_7, \tilde{\Psi}_7\}$ and all indices transform under the fundamental representation of the unbroken $SO(7)$. In order to better monitor how the results depend on the multiplicity of NGBs and fermions, we perform the calculation for a generic $SO(N)/SO(N-1)$ coset with N_f composite fermions ψ in the fundamental of $SO(N-1)$. Taking $N = 8$ and $N_f = 2 \times 3 = 6$ thus reproduces the simplified model of Sec. III A.

The perturbative limits are obtained by first expressing the scattering amplitudes in terms of components with definite $SO(N-1)$ quantum numbers. In the case of $SO(7)$ the product of two fundamentals decomposes as $\mathbf{7} \otimes \mathbf{7} = \mathbf{1} \oplus \mathbf{21}_a \oplus \mathbf{27}_s$, where the indices a and s label respectively the antisymmetric and symmetric two-index representations. A completely analogous

decomposition holds in the general case of $SO(N)/SO(N-1)$,[19] but for simplicity we will use the $SO(7)$ notation in the following to label the various components. The leading tree-level contributions to the scattering amplitudes arise from the contact interaction generated by the expansion of the NGB kinetic term of Eq. (3.4) and from the NGB-fermion interactions of Eq. (3.9). The structure of the corresponding vertices implies that the four-NGB amplitude has components in all three irreducible representations of $SO(N-1)$ and contains all partial waves. The amplitude with two NGBs and two fermions, instead, has only the antisymmetric component of $SO(N-1)$ and starts with the p-wave. At energies much larger than all masses the amplitudes read

$$\begin{aligned}
\mathcal{M}(\pi^a\pi^b \to \pi^c\pi^d) &= \frac{s}{f^2}\delta^{ab}\delta^{cd} + \frac{t}{f^2}\delta^{ac}\delta^{bd} + \frac{u}{f^2}\delta^{ad}\delta^{bc},\\
\mathcal{M}(\pi^a\pi^b \to \bar{\Psi}^c_{7_L}\Psi^d_{7_L}) &= \frac{s}{2f^2}\sin\theta(\delta^{ac}\delta^{bd} - \delta^{ad}\delta^{bc}),\\
\mathcal{M}(\pi^a\pi^b \to \bar{\Psi}^c_{7_R}\Psi^d_{7_R}) &= \frac{s}{2f^2}\sin\theta(\delta^{ac}\delta^{bd} - \delta^{ad}\delta^{bc}).
\end{aligned} \tag{G1}$$

They decompose into irreducible representations of $SO(N-1)$ as follows:

$$\begin{aligned}
\mathcal{M}^{(\mathbf{1})}(\pi^a\pi^b \to \pi^c\pi^d) &= (N-2)\tfrac{s}{f^2},\\
\mathcal{M}^{(\mathbf{21})}(\pi^a\pi^b \to \pi^c\pi^d) &= \tfrac{s}{f^2}\cos\theta,\\
\mathcal{M}^{(\mathbf{27})}(\pi^a\pi^b \to \pi^c\pi^d) &= -\tfrac{s}{f^2},\\
\mathcal{M}^{(\mathbf{21})}(\pi^a\pi^b \to \bar{\Psi}^c_{7_L}\Psi^d_{7_L}) &= \tfrac{s}{2f^2}\sin\theta,\\
\mathcal{M}^{(\mathbf{21})}(\pi^a\pi^b \to \bar{\Psi}^c_{7_R}\Psi^d_{7_R}) &= \tfrac{s}{2f^2}\sin\theta.
\end{aligned} \tag{G2}$$

Performing a partial wave decomposition we get

$$\mathcal{M}^{(\mathbf{r})} = \sum_{\lambda_i,\lambda_f}\mathcal{M}^{(\mathbf{r})}_{\lambda_i,\lambda_f} = 16\pi k^{(i)}k^{(f)}\sum_{j=0}^{\infty}a_j^{(\mathbf{r})}(2j+1) \times \sum_{\lambda_i,\lambda_f}D^j_{\lambda_i,\lambda_f}(\theta), \tag{G3}$$

where λ_i, λ_f are the initial and final state total helicities, and $k^{(i)}(k^{(f)})$ is equal to either 1 or $\sqrt{2}$ depending on whether the two particles in the initial (final) state are distinguishable or identical respectively. In the above equation $\mathcal{M}^{(\mathbf{r})}$ should be considered as a matrix acting on the space of different channels. The coefficients $a_j^{(\mathbf{r})}$ are given by

$$a_j^{(\mathbf{r})} = \frac{1}{32\pi k^{(i)}k^{(f)}}\int_0^\pi d\theta \sum_{\lambda_i,\lambda_f}\mathcal{D}^j_{\lambda_i,\lambda_f}(\theta)\mathcal{M}^{(\mathbf{r})}_{\lambda_i,\lambda_f}. \tag{G4}$$

and act as matrices on the space of (elastic and inelastic) channels with total angular momentum j and $SO(N-1)$ irreducible representations $\mathbf{r}$. They can be rewritten as a function of the scattering phase as

$$a_j^{(\mathbf{r})} = \frac{e^{2i\delta_j^{(\mathbf{r})}}-1}{2i} \sim \delta_j^{(\mathbf{r})}. \tag{G5}$$

Our NDA estimate of the perturbativity bound is derived by requiring this phase to be smaller than maximal:

$$|\delta_j^{(\mathbf{r})}| < \frac{\pi}{2} \Rightarrow |a_j^{(\mathbf{r})}| < \frac{\pi}{2} \tag{G6}$$

Let us consider first the case $\mathbf{r} = \mathbf{1}$, corresponding to the amplitude singlet of $SO(N-1)$. The only contribution comes from the four-NGB channel. Since the helicities of the initial and final states are all zeros, in this particular case the Wigner functions $\mathcal{D}^j_{\lambda_i,\lambda_f}(\theta)$ reduce to the Legendre polynomials:

$$a_j^{(\mathbf{1})} = \frac{1}{64\pi}\int_0^\pi d\theta P_j(\cos\theta)\mathcal{M}^{(\mathbf{1})}. \tag{G7}$$

The first and strongest perturbativity constraint comes from the s-wave amplitude, which corresponds to $j = 0$. We find:

$$a_0^{(\mathbf{1})} = \frac{N-2}{32\pi}\frac{s}{f^2}, \tag{G8}$$

where $N = 8$ in our case. From Eqs. (G6) and (G8), one obtains the constraint of Eq. (3.15).

We analyze now the constraint from the scattering in the antisymmetric representation, $\mathbf{r} = \mathbf{21}$. In this case, both the NGB and the fermion channels contribute; the process $\pi\pi \to \pi\pi$ is however independent of the fermion and Goldstone multiplicities and can be neglected in the limit of N and N_f. The process involving fermions is a function of N_f and generates a perturbative limit which is comparable and complementary to the previous one. We have:

[19] One has $\mathbf{N}\otimes\mathbf{N} = \mathbf{1}\oplus[\mathbf{N(N-1)/2}]_a\oplus[\mathbf{N(N+1)/2-1}]_s$.

$$a_j^{(\mathbf{21})} = \sum_{\lambda_f=\pm 1} \frac{1}{32\pi} \int_0^\pi d\theta \mathcal{D}^j_{0,\lambda_f}(\theta) \mathcal{M}^{(\mathbf{21})}_{0,\lambda_f}. \quad \text{(G9)}$$

As anticipated, this equation vanishes for $j = 0$, so that the strongest constraint is now derived for p-wave scattering, with $j = 1$. We have

$$a_1^{(\mathbf{21})} = \frac{N_f}{24\sqrt{2}\pi} \frac{s}{f^2}. \quad \text{(G10)}$$

From Eqs. (G6) and (G10) follows the constraint of Eq. (3.16).

[1] Z. Chacko, H.-S. Goh, and R. Harnik, The Twin Higgs: Natural Electroweak Breaking from Mirror Symmetry, Phys. Rev. Lett. **96**, 231802 (2006).
[2] R. Barbieri, T. Gregoire, and L. J. Hall, Mirror world at the large hadron collider, arXiv:hep-ph/0509242.
[3] Z. Chacko, Y. Nomura, M. Papucci, and G. Perez, Natural little hierarchy from a partially Goldstone twin Higgs, J. High Energy Phys. 01 (2006) 126.
[4] Z. Chacko, H.-S. Goh, and R. Harnik, A twin Higgs model from left-right symmetry, J. High Energy Phys. 01 (2006) 108.
[5] S. Chang, L. J. Hall, and N. Weiner, A supersymmetric twin Higgs, Phys. Rev. D **75**, 035009 (2007).
[6] P. Batra and Z. Chacko, A composite twin Higgs model, Phys. Rev. D **79**, 095012 (2009).
[7] N. Craig and K. Howe, Doubling down on naturalness with a supersymmetric twin Higgs, J. High Energy Phys. 03 (2014) 140.
[8] N. Craig, S. Knapen, and P. Longhi, Neutral Naturalness from Orbifold Higgs Models, Phys. Rev. Lett. **114**, 061803 (2015).
[9] M. Geller and O. Telem, Holographic Twin Higgs Model, Phys. Rev. Lett. **114**, 191801 (2015).
[10] G. Burdman, Z. Chacko, R. Harnik, L. de Lima, and C. B. Verhaaren, Colorless top partners, a 125 GeV Higgs, and the limits on naturalness, Phys. Rev. D **91**, 055007 (2015).
[11] N. Craig, S. Knapen, and P. Longhi, The orbifold Higgs, J. High Energy Phys. 03 (2015) 106.
[12] N. Craig, A. Katz, M. Strassler, and R. Sundrum, Naturalness in the dark at the LHC, J. High Energy Phys. 07 (2015) 105.
[13] R. Barbieri, D. Greco, R. Rattazzi, and A. Wulzer, The composite twin Higgs scenario, J. High Energy Phys. 08 (2015) 161.
[14] M. Low, A. Tesi, and L.-T. Wang, The twin Higgs mechanism and composite Higgs, J. High Energy Phys. 03 (2016) 108.
[15] D. Curtin and P. Saraswat, Towards a no-lose theorem for naturalness, Phys. Rev. D **93**, 055044 (2016).
[16] C. Csaki, M. Geller, O. Telem, and A. Weiler, The flavor of the composite twin Higgs, J. High Energy Phys. 09 (2016) 146.
[17] N. Craig, S. Knapen, P. Longhi, and M. Strassler, The vector-like twin Higgs, J. High Energy Phys. 07 (2016) 002.
[18] R. Harnik, K. Howe, and J. Kearney, Tadpole-induced electroweak symmetry breaking and pNGB Higgs models, J. High Energy Phys. 03 (2017) 111.
[19] R. Barbieri, L. J. Hall, and K. Harigaya, Minimal mirror twin Higgs, J. High Energy Phys. 11 (2016) 172.
[20] Z. Chacko, N. Craig, P. J. Fox, and R. Harnik, Cosmology in mirror twin Higgs and neutrino masses, J. High Energy Phys. 07 (2017) 023.
[21] N. Craig, S. Koren, and T. Trott, Cosmological signals of a mirror twin Higgs, J. High Energy Phys. 05 (2017) 038.
[22] A. Katz, A. Mariotti, S. Pokorski, D. Redigolo, and R. Ziegler, SUSY meets her twin, J. High Energy Phys. 01 (2017) 142.
[23] D. B. Kaplan, Flavor at SSC energies: A new mechanism for dynamically generated fermion masses, Nucl. Phys. **B365**, 259 (1991).
[24] G. Aad *et al.* (ATLAS, CMS Collaboration), Measurements of the Higgs boson production and decay rates and constraints on its couplings from a combined ATLAS and CMS analysis of the LHC pp collision data at $\sqrt{s} = 7$ and 8 TeV, J. High Energy Phys. 08 (2016) 045.
[25] A. Thamm, R. Torre, and A. Wulzer, Future tests of Higgs compositeness: Direct vs indirect, J. High Energy Phys. 07 (2015) 100.
[26] M. Ciuchini, E. Franco, S. Mishima, and L. Silvestrini, Electroweak precision observables, new physics and the nature of a 126 GeV Higgs boson, J. High Energy Phys. 08 (2013) 106.
[27] J. de Blas, M. Ciuchini, E. Franco, S. Mishima, M. Pierini, L. Reina, and L. Silvestrini, *Proc. Sci.*, ICHEP2016 (2017) 690 [arXiv:1611.05354].
[28] C. Anastasiou, E. Furlan, and J. Santiago, Realistic composite Higgs models, Phys. Rev. D **79**, 075003 (2009).
[29] C. Grojean, O. Matsedonskyi, and G. Panico, Light top partners and precision physics, J. High Energy Phys. 10 (2013) 160.
[30] D. Ghosh, M. Salvarezza, and F. Senia, Extending the analysis of electroweak precision constraints in composite Higgs models, Nucl. Phys. **B914**, 346 (2017).
[31] G. F. Giudice, C. Grojean, A. Pomarol, and R. Rattazzi, The strongly-interacting light Higgs, J. High Energy Phys. 06 (2007) 045.
[32] R. Barbieri, B. Bellazzini, S. Rychkov, and A. Varagnolo, The Higgs boson from an extended symmetry, Phys. Rev. D **76**, 115008 (2007).
[33] A. De Simone, O. Matsedonskyi, R. Rattazzi, and A. Wulzer, A first top partner's hunter guide, J. High Energy Phys. 04 (2013) 004.
[34] ATLAS Collaboration, Report No. ATLAS-CONF-2016-101, 2016.

[35] CMS Collaboration, Report No. CMS-PAS-B2G-16-011, 2016, [Inspire].
[36] A. Kagan, Talk at *KITP workshop on Physics of the Large Hadron Collider* (unpublished); Talk at *Naturalness 2014*, Weizmann Institute (unpublished); Talk at *Physics from Run 2 of the LHC, 2nd NPKI Workshop*, Jeju (unpublished).
[37] J. Galloway, M. A. Luty, Y. Tsai, and Y. Zhao, Induced electroweak symmetry breaking and supersymmetric naturalness, Phys. Rev. D **89**, 075003 (2014).
[38] S. Chang, J. Galloway, M. Luty, E. Salvioni, and Y. Tsai, Phenomenology of induced electroweak symmetry breaking, J. High Energy Phys. 03 (2015) 017.
[39] J. Mrazek, A. Pomarol, R. Rattazzi, M. Redi, J. Serra, and A. Wulzer, The other natural two Higgs doublet model, Nucl. Phys. **B853**, 1 (2011).
[40] R. Contino and A. Pomarol, Holography for fermions, J. High Energy Phys. 11 (2004) 058.
[41] S. Coleman, J. Wess, and B. Zumino, Structure of phenomenological Lagrangians. I, Phys. Rev. **177**, 2239 (1969).
[42] C. G. Callan, S. Coleman, J. Wess, and B. Zumino, Structure of phenomenological Lagrangians. II, Phys. Rev. **177**, 2247 (1969).
[43] R. Contino, D. Marzocca, D. Pappadopulo, and R. Rattazzi, On the effect of resonances in composite Higgs phenomenology, J. High Energy Phys. 10 (2011) 081.
[44] G. Panico and A. Wulzer, The discrete composite Higgs model, J. High Energy Phys. 09 (2011) 135.
[45] R. Contino and M. Salvarezza, One-loop effects from spin-1 resonances in composite Higgs models, J. High Energy Phys. 07 (2015) 065.
[46] D. Greco and K. Mimouni, The RG-improved twin Higgs effective potential at NNLL, J. High Energy Phys. 11 (2016) 108.
[47] R. Barbieri, A. Pomarol, R. Rattazzi, and A. Strumia, Electroweak symmetry breaking after LEP1 and LEP2, Nucl. Phys. **B703**, 127 (2004).
[48] B. Grinstein and M. B. Wise, Operator analysis for precision electroweak physics, Phys. Lett. B **265**, 326 (1991).
[49] M. E. Peskin and T. Takeuchi, A New Constraint on a Strongly Interacting Higgs Sector, Phys. Rev. Lett. **65**, 964 (1990).
[50] M. E. Peskin and T. Takeuchi, Estimation of oblique electroweak corrections, Phys. Rev. D **46**, 381 (1992).
[51] R. Contino and M. Salvarezza, Dispersion relations for electroweak observables in composite Higgs models, Phys. Rev. D **92**, 115010 (2015).
[52] K. Agashe, R. Contino, L. Da Rold, and A. Pomarol, A custodial symmetry for $Zb\bar{b}$", Phys. Lett. B **641**, 62 (2006).
[53] J. Elias-Miro, J. R. Espinosa, E. Masso, and A. Pomarol, Higgs windows to new physics through $d = 6$ operators: constraints and one-loop anomalous dimensions, J. High Energy Phys. 11 (2013) 066.
[54] R. Rattazzi, Phenomenological implications of a heavy isosinglet up type quark, Nucl. Phys. **B335**, 301 (1990).
[55] M. Carena, E. Ponton, J. Santiago, and C. E. M. Wagner, Electroweak constraints on warped models with custodial symmetry, Phys. Rev. D **76**, 035006 (2007).
[56] M. Gillioz, A light composite Higgs boson facing electroweak precision tests, Phys. Rev. D **80**, 055003 (2009).
[57] C. Patrignani *et al.* (Particle Data Group Collaboration), Review of particle physics, Chin. Phys. C **40**, 100001 (2016).
[58] T. Golling *et al.*, Physics at a 100 TeV pp collider: Beyond the standard model phenomena, arXiv:1606.00947.
[59] O. Matsedonskyi, G. Panico, and A. Wulzer, Top partners searches and composite Higgs models, J. High Energy Phys. 04 (2016) 003.
[60] O. Matsedonskyi, G. Panico, and A. Wulzer, Light top partners for a light composite Higgs, J. High Energy Phys. 01 (2013) 164.
[61] D. Marzocca, M. Serone, and J. Shu, General composite Higgs models, J. High Energy Phys. 08 (2012) 013.
[62] A. Pomarol and F. Riva, The composite Higgs and light resonance connection, J. High Energy Phys. 08 (2012) 135.
[63] D. Pappadopulo, A. Thamm, and R. Torre, A minimally tuned composite Higgs model from an extra dimension, J. High Energy Phys. 07 (2013) 058.
[64] D. Buttazzo, F. Sala, and A. Tesi, Singlet-like Higgs bosons at present and future colliders, J. High Energy Phys. 11 (2015) 158.
[65] G. Degrassi, S. Di Vita, J. Elias-Miro, J. R. Espinosa, G. F. Giudice, G. Isidori, and A. Strumia, Higgs mass and vacuum stability in the standard model at NNLO, J. High Energy Phys. 08 (2012) 098.
[66] G. Altarelli and R. Barbieri, Vacuum polarization effects of new physics on electroweak processes, Phys. Lett. B **253**, 161 (1991).
[67] G. Altarelli, R. Barbieri, and S. Jadach, Toward a model independent analysis of electroweak data, Nucl. Phys. **B369**, 3 (1992); Erratum, Nucl. Phys. **B376**, 444 (1992).
[68] G. Altarelli, R. Barbieri, and F. Caravaglios, Nonstandard analysis of electroweak precision data, Nucl. Phys. **B405**, 3 (1993).
[69] M. Ciuchini, E. Franco, S. Mishima, M. Pierini, L. Reina, and L. Silvestrini, Update of the electroweak precision fit, interplay with Higgs-boson signal strengths and model-independent constraints on new physics, Phys. Procedia **273–275**, 2219 (2016).